Available online at www.sciencedirect.com
ScienceDirect
Journal of Sound and Vibration 310 (2008) 558–586
JOURNAL OF SOUND AND VIBRATION
www.elsevier.com/locate/jsvi

Nonlinear interaction between a moving vehicle and a plate elastically mounted on a tunnel

K. Müller[a,*], H. Grundmann[a], S. Lenz[b]

[a]*Chair of Structural Mechanics, Technische Universität München, Germany*
[b]*Linde Engineering Division, The Linde Group, Höllriegelskreuth, Germany*

Received 13 December 2006; received in revised form 19 October 2007; accepted 22 October 2007
Available online 11 December 2007

Abstract

The paper presents a theoretical study of the interaction between a nonlinear model of a moving vehicle (velocity v) and a plate elastically mounted in a tunnel. An efficient approach to the solution of the problem of *vehicle–slab-track–tunnel– soil* interaction is developed on the basis of a coupling of the Finite Element and Integral Transform methods (FEM and ITM). According to this approach the tunnel which may have an arbitrary shape and a portion of the surrounding soil is modelled by Finite Elements while the soil (half-space) is described by the ITM. The corresponding solution is found using the solutions for the uniform half-space and for the continuum with a cylindrical cavity. To exploit the invariance of the structure in longitudinal direction x, for this direction additionally to the time–frequency transform ($t\circ\!\!-\!\!\bullet\omega$) a space–wavenumber transform ($x\circ\!\!-\!\!\bullet k_x$) is used. The case of a half-space is analyzed using a Fourier transform also in the second horizontal direction ($y\circ\!\!-\!\!\bullet k_y$) and an analytical solution for the z-direction on the basis of exponential functions. In the case of the infinite continuum with the cavity a Fourier series (for the circumferential direction) and a series of cylindrical functions (for the radial direction) are used for the solution regarding the cross-sectional coordinates (y, z). The tunnel structure, that may have an arbitrary shape, and a portion of the surrounding soil will be modelled by Finite Elements in a ($x\circ\!\!-\!\!\bullet k_x, t\circ\!\!-\!\!\bullet\omega$) transformed domain.

In order to observe the boundary conditions at the surface of the half-space as well as at the surface of the cavity, the superposition of the two solutions has to be performed after an inverse Fourier transform (IFT) in the (k_x, y, z, ω)-domain.

The solution for the complete system *floating slab-track–tunnel–half-space* is obtained in the (k_x, y, z, ω)-domain. Once the system transfer function $H(\omega')$ (with $\omega' = \omega + vk_x$) for this complete coupled system is found, the displacements of the plate can be calculated in time domain by the IFT of the product $p(\omega')H(\omega')$, i.e. the convolution of the loading $p(t)$ with the impulse response function $h(t)$, which completely represents the behavior of the coupled system. In the context of the coupling of systems in a relative movement the problems of differential algebraic equations (DAE) have to be observed.

1. Introduction and overview of existing models

The investigation of the radiation of vibrations in the elastic-isotropic half-space caused by loads moving in cavities of arbitrary geometry plays an important role for underground railway constructions when designing

*Corresponding author. Tel.: +49 89 289 28341; fax: +49 89 289 28665.
E-mail address: kai.mueller@mytum.de (K. Müller).

0022-460X/$ - see front matter
doi:10.1016/j.jsv.2007.10.042

measures on the track, like ballast mats, elastically mounted sleepers, resilient mats or floating slab-tracks (mass–spring systems). In the case of mass–spring systems especially the interaction between the dynamic behavior of the elastically mounted plate and its support is of interest.

For the uniform half-space subjected to dynamic surface loadings and for the interaction of the half-space with structures at its surface or at excavations a large number of solutions has been published. An overview is given by Grundmann [1]. Some recent publications that deal with the description of the variation of the stresses across the interface for a beam resting on a half-space shall be added. Postulating compatibility across the interface, Lombaert et al. [2], Grundmann and Lenz [3], Auersch [4], François et al. [5], Andersen and Jones [6], Karlström and Boström [7] and Steenbergen and Metrikine [8] describe the stress variability with the aid of local or global shape functions.

For the dynamic investigation of a tunnel different approaches are well established. Along with simple analytical models, these are the Finite Element Method (FEM), the Thin Layer Method (TLM), the Boundary Element Method (BEM) and the Integral Transform Method (ITM). Due to the restrictions of the different methods also hybrid methods have been developed, that combine two of the above-mentioned methods, as e.g. a coupled FEM–BEM approach. In the following a short overview of those methods in relation to tunnel dynamics shall be given.

One of the earliest publications presenting an analytical solution for the vibration from underground railway systems was presented by Krylov [9]. However, the application of this model was restricted to vibrations in a very low-frequency range (1–4 Hz), because the model neglected the influence of the diameter of the tunnel assuming that it was small compared to the characteristic wave lengths of the vibration spectra. An approximate solution to the problem taking into account the diameter of the tunnel and thus also valid for frequencies higher than 4 Hz on the basis of the reciprocity principle is given by Lin and Krylov [10]. Rücker and Said [11] use a two-dimensional (2D) FEM model to solve the tunnel–soil–interaction problem by the use of local, absorbing boundary conditions in vertical direction and by the aid of the TLM in horizontal direction. A model presented by Metrikine and Vrouwenvelder [12] consists of two 2D viscoelastic layers representing the soil below and above the tunnel and two identical beams by which the tunnel is modelled. The beams are connected by continuously distributed springs. This model can account for the moving loads and the wave propagation in longitudinal direction, but the wave propagation in the transversal direction cannot be included. Jones et al. [13,14] developed a coupled 2D FEM–BEM approach to model both a bored, circular lined and unlined tunnel and a cut-and-cover tunnel of a rectangular cross-section with and without extra foundation engineering. Hussein and Hunt [15,16] and Forrest and Hunt [17,18] present a half-analytical model on the basis of the cylinder theory, which is capable of dealing with the three dimensional (3D) dynamic interaction between track, tunnel and soil as well as with the wave propagation into the surrounding soil. By the use of this method Hussein has investigated the insertion loss of a floating slab-track for four different geometric situations of the elastic support [15]. This approach uses the solution for the continuum with a cylindrical cavity that also is one part of the method shown in this paper. By this approach the soil and the tunnel are modelled as a viscoelastic full-space with an infinitely long thin cylindrical tunnel shell utilizing the theory of Flügge [19]. The complete system is also assumed to be invariant in longitudinal direction. The equilibrium equations are formulated then in the wavenumber–frequency domain. Though such an analytical model is very efficient with respect to computation time, its applicability is limited. It can be applied only if the tunnel has a circular cross-section, lies far below the ground surface and the soil is not stratified.

All the above-mentioned models either are 2D and thus not capable of modelling the wave propagation in the lateral direction or they treat the soil as a full-space and thus cannot take into account the wave reflections at the surface of the soil or they imply restrictions concerning the geometry of the cross-section of the tunnel structure and thus cannot account for the influences of different tunnel structures. Andersen and Jones [6] compare 2D and 3D coupled FEM–BEM models for a cut-and-cover double-track tunnel and a deep single-track tunnel dug with the New Austrian Tunneling Method (NATM), calculating surface ground vibration up to 80 Hz for loads applied directly to the tunnel invert. Their conclusion is that for absolute vibration transmission predictions and more accurate estimates of the effects in response due to changes in tunnel structure and depth 3D models are required.

A general 3D coupled FEM–BEM model has been developed by Andersen and Jones [20], which however is very costly with respect to the computational effort.

In order to overcome those computational drawbacks so-called "2.5D" methods have been developed assuming that the cross-section of the complete system is invariant in longitudinal direction. Discretization with the combined FEM–BEM method is only required over the cross-section, which can therefore be of arbitrary geometry, while a Fourier transform is applied longitudinally to describe the problem depending on discrete wavenumbers in that direction. In Ref. [21] Sheng et al. use this approach to model the vibration from both a surface railway on layered soil and a bored tunnel. Sheng et al. [22] have presented a prediction model for soil vibrations due to stationary or moving harmonic loads acting in a circular tunnel with or without lining in layered ground. Instead of FEM–BEM coupling the authors apply the *Discrete Wavenumber-Fictitious Force Method*, utilizing moving Green's functions for a layered half-space as well as for a radially layered cylinder of infinite length in order to formulate the boundary integral equation along the tunnel-soil interface. Though for the boundary integral equation introduced by Luco and de Barros [23] one needs—as for the conventional BEM—not only the displacements Green's functions, but also the Green's functions for the stresses, by treating the inner domain (a cylinder of infinite length) as a substructure, only the displacements Green's functions are needed for the displacements of the soil, the tunnel structure and the cylinder. Due to the fact that the calculation of the Green's functions for the layered ground is very costly the *Discrete Wavenumber FEM–BEM Method* proposed by Sheng et al. [24] has turned out to be more efficient.

Within the scope of the EU-project CONVURT (CONtrol of Vibrations from Underground Rail Traffic) Clouteau et al. [25] and Degrande et al. [26] followed a slightly different approach, assuming periodicity rather than invariance in the longitudinal direction. The periodicity of the tunnel and the soil is accounted for by the application of the *Floquet transform* instead of a *Fourier* one, which allows to restrict the discretization to only one single reference cell which represents a structural section of the tunnel. By this approach one can use the 3D BEM-technique for layered soil, because the periodic Green's kernels exhibit the same singularities as the 3D Green's functions [27]. This is an advantage compared with the so-called 2.5D FEM–BEM methods, which assume a translation invariant model and require the repeated calculation of all singularities after the Fourier transform along the tunnel axis, except for trains running on the surface of the half-space, where the singular stress kernels vanish [28]. Theoretical results for a shallow cut-and-cover masonry tunnel embedded in layers of sand in Paris and for a deep bored tunnel with periodic cast-iron lining in London clay are given in Ref. [26], while detailed measurements of train, track, tunnel, soil and building vibration for the London site can be found in Ref. [29].

In Ref. [30] Grundmann and Müller calculated by the approach described in this paper the vibrations of a tunnel in the homogeneous full-space using three different methods. A thin tunnel shell has been modelled by the solution for the radially layered full-space with an infinitely long cylindrical cavity as well as by the application of the theory of Flügge [19] and by the aid of Finite Elements.

The aim of this paper is to develop a mechanical model which is capable of describing the dynamics of an underground railway tunnel embedded in the half-space. The model can easily account for interior constructions in order to model a floating slab-track system. So the approach allows to calculate the complete 3D interaction problem of the system *vehicle–floating slab-track–tunnel–soil*.

In the case of a tunnel embedded in the half-space one has to account for the finite extension of the tunnel structure in the cross-sectional plane and its infinite extension in the longitudinal direction as well as for the infinite extensions of the soil in both horizontal and in the vertical direction. Under those circumstances the direct use of the ITM is impossible, because this method only allows to take into account the full or layered half-space or the radially layered continuum with a cylindrical cavity. The description of such a problem can be achieved in an advantageous manner by a coupling of the FEM with either the BEM [31] or the ITM [32,1,33]. The proposed method describes a synthesis of a modified FEM description in transformed (k_x, ω)-domain and the ITM, with FEM to take into account the finite cross-section of the tunnel structure and with BEM or ITM to consider the infinite extensions of the soil.

The solution technique is not restricted to cylindrical tunnel shells but applicable to any arbitrary shape of the tunnel (Fig. 1). Then one has to work with a *fictitious* internal cylindrical surface Γ_s of the continuum—a contour where later the contact of the half-space with cylindrical cavity to the interior FEM mesh has to be established—and an interior FEM domain, not only for the tunnel itself but also for the soil between the

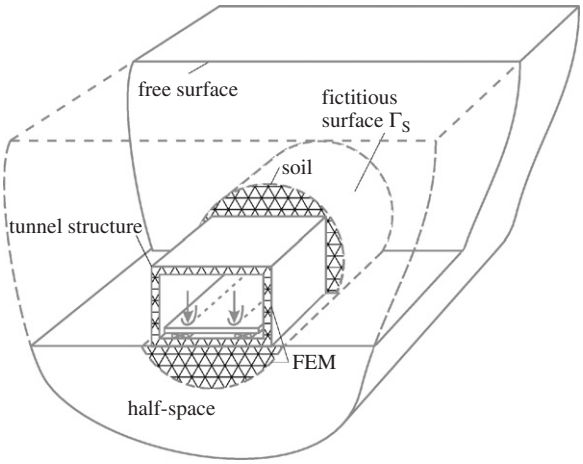

Fig. 1. Half-space with tunnel structure.

tunnel and the surface Γ_s. In the figure the rectangular tunnel structure and a portion of the adjacent soil are modelled by Finite Elements in the Fourier transformed (k_x, ω)-domain.

The infinite domain outside the FEM-regime will be described by a semi-analytical approach using the equations of the elastic isotropic continuum. The final solution for the half-space with a cylindrical cavity is constructed by a superposition of a response which starts at the internal cylindrical surface Γ_s and a solution which originates at the plane surface of the half-space. For the description of the former serves the solution for the continuum with a cylindrical cavity in polar coordinates. For the latter serves the solution for the half-space in cartesian coordinates y and z, caused by stress-states at the upper surface of the half-space. In the case of the infinite continuum with cylindrical cavity a general form of the solution results if a Fourier series representation for its variation in the circumferential direction is introduced. This leads to the description of the behavior in the radial direction by cylinder functions, where their specific form depends on the dilatational and shear wave velocities, the frequency ω, the wavenumber k_x and the velocity v of the moving load. The half-space is described in a Fourier transformed (k_x, k_y, z, ω)-domain. In order to observe the boundary conditions at the surface of the half-space as well as at the surface of the cavity, the superposition of the two solutions has to be performed, after an inverse Fourier transform (IFT), in the (k_x, y, z, ω)-domain.

The generated solutions are taken as a basis for the investigation of the coupled system *tunnel structure–half-space with cylindrical cavity*. In order to keep the computational effort low, it is advantageous to use an adequately composed form of the Finite Elements, i.e. FE in a transformed domain. This means that the equations in the FEM domain have to be subjected to a two-fold integral transform, specifically for the time–frequency ($t \circ\!\!-\!\!\bullet \omega$) and the space–wavenumber ($x \circ\!\!-\!\!\bullet k_x$) transition ($x$ stands for the coordinate in the longitudinal direction of the tunnel). In the transformed (k_x, y, z, ω)-domain, as far as the (y, z)-domain is concerned, one works with usual FEM discretization techniques. The respective stiffness matrix is derived by the use of the Parseval's theorem. An advantageous approach specifically for the ITM–FEM coupling in a 2D problem was proposed in Ref. [32]. It was generalized in the meantime by Grundman and Dinkel [34] for 3D line structures and by Rastandi [33] for the 3D situation of an excavation at the surface of a half-space. The above-described approach is illustrated in more detail in Ref. [35].

Once the system transfer function $H(\omega')$ (with $\omega' = \omega + vk_x$) for the system consisting of the plate on an elastic foundation mounted on the tunnel is found, the displacement of the plate at the point $x = vt$ can be calculated in the moving coordinate system by the IFT of the product $p(\omega')H(\omega')$, which in the original time domain corresponds to a convolution of the loading $p(t)$ with the impulse response function $h(t)$. The latter is calculated by the IFT of the system transfer function $H(\omega')$ and represents completely the behavior of the coupled system *floating slab track– tunnel– half-space* [3]. In the context of the coupling of systems in a relative movement the problems of differential algebraic equations (DAE) have to be observed [36].

This paper is structured as follows. In Section 2 the solutions for a uniform half-space and for a continuum with a cylindrical cavity will be discussed. In Section 3 the solution for the half-space with a cylindrical cavity is developed and the derivation of a matrix characterizing the force-displacement behavior of this system at the cylindrical surface Γ_s by the use of an energy approach is shown. After that in Section 4 the FEM in the wavenumber/frequency domain is presented. The interaction of a mass–spring system with a nonlinear single-degree-of-freedom (sdof) system will be described in Section 5. Here special problems that may arise at the nonlinear interaction and how to overcome them will be discussed. In Section 6 some numerical results for the case of a nonlinear model of the moving bogie with different wheel out-of-roundnesses at the two wheels are presented. Finally, in Section 7 some closing statements are given.

2. Basic equations of continuum dynamics and their solutions

The solution for the half-space with cylindrical cavity will be found as a superposition of the solution for a uniform half-space and the solution for a continuum with a cylindrical cavity. Therefore, in this chapter those two solutions are described. As shown in Ref. [1] it is favorable to derive both these solutions on the basis of the ITM.

The governing equation of continuum dynamics is given by the Lamé's equation of elastodynamics representing a system of three coupled partial differential equations (PDE)

$$\mu u^i|^j_j + (\lambda+\mu)u^j|^i_j - \rho\ddot{u}^i = 0, \tag{1}$$

with $|_i$ as covariant derivation, u^i as the displacements, μ and λ as Lamé's constants and ρ as the density of the material. In the general case one can approximately account for material damping by considering the Lamé's constants μ and λ as complex quantities

$$\lambda = \lambda'(1 + \mathrm{i}\,\mathrm{sign}(\omega)\zeta), \tag{2}$$

$$\mu = \mu'(1 + \mathrm{i}\,\mathrm{sign}(\omega)\zeta), \tag{3}$$

provided that the time and frequency domains are related by the following Fourier transform:

$$f(t) = \frac{1}{2\pi}\int_{-\infty}^{+\infty} \hat{f}(\omega)\mathrm{e}^{\mathrm{i}\omega t}\,\mathrm{d}\omega. \tag{4}$$

2.1. Half-space solution

In order to construct the solution for a half-space with a cylindrical cavity as a first step it is customary to calculate the solution for the full or layered half-space without any cavity. As mentioned before this task shall be performed with the aid of the ITM.

By the use of the decomposition of Helmholtz into a scalar potential Φ and a vectorial potential Ψ_k

$$u^i = \Phi^i + \Psi_k|_j \varepsilon^{ijk}, \tag{5}$$

the system of 3 coupled PDE given by Lamé's equation of elastodynamics (1) changes into a system of 4 wave equations that are decoupled in the case the components Ψ_k are given with respect to the cartesian coordinate system:

$$\Phi|^j_j - \frac{\rho}{\lambda+2\mu}\ddot{\Phi} = 0, \tag{6}$$

$$\Psi_i|^j_j - \frac{\rho}{\mu}\ddot{\Psi}_i = 0. \tag{7}$$

The quantities $c_p = \sqrt{(\lambda+2\mu)/\rho}$ and $c_s = \sqrt{\mu/\rho}$ can be interpreted as velocities of the dilatational and the shear waves, respectively.

In the case of cartesian coordinates one can easily see that the matrix of the differential operators that have to be applied to the vectorial potential Ψ_i in Eq. (7) is singular, so the components of the vectorial potential are linearly dependent and consequently one component can be arbitrarily chosen. In the following it is assumed that $\Psi_z = 0$ (the completeness of this approach has been proved in general by Long [37]).

If one applies a threefold Fourier transform ($x\circ\!\!-\!\!\bullet k_x, y\circ\!\!-\!\!\bullet k_y, t\circ\!\!-\!\!\bullet\omega$), Eqs. (6) and (7) transform into a system of 3 decoupled ordinary differential equations (ODE) (the hat ($\hat{..}$) indicates quantities in the Fourier transformed domain).

$$\left(-k_x^2 - k_y^2 + \frac{\omega^2}{c_p^2}\right)\hat{\Phi} + \frac{\partial^2\hat{\Phi}}{\partial z^2} = 0, \tag{8}$$

$$\left(-k_x^2 - k_y^2 + \frac{\omega^2}{c_s^2}\right)\hat{\Psi}_i + \frac{\partial^2\hat{\Psi}_i}{\partial z^2} = 0, \quad i = x, y. \tag{9}$$

Now it is an easy task to find the corresponding solution in the Fourier transformed (k_x, k_y, z, ω)-domain, which is given by an exponential approach with the unknown coefficients A_j and B_{ij}

$$\hat{\Phi} = A_1 e^{\lambda_1 z} + A_2 e^{-\lambda_1 z}, \tag{10}$$

$$\hat{\Psi}_i = B_{i1} e^{\lambda_2 z} + B_{i2} e^{-\lambda_2 z} \tag{11}$$

with

$$\lambda_1^2 = k_x^2 + k_y^2 - k_p^2, \tag{12}$$

$$\lambda_2^2 = k_x^2 + k_y^2 - k_s^2 \tag{13}$$

and

$$k_p = \frac{\omega}{c_p}, \quad k_s = \frac{\omega}{c_s}. \tag{14}$$

In principal for the case of the infinite half-space the radiation condition of Sommerfeld, that means that waves can only propagate from and not to the source of excitation, has to be observed. It has been shown in Ref. [38] (the authors are not aware of any publication in English, in which this information can be found) that if one only works with $\omega < 0$, the radiation condition of Sommerfeld will be always—also in the general case taking into account material damping by the use of complex Lamé's constants—observed by setting $A_1 = B_{i1} = 0$. In this context one has to work with the positive real or the positive imaginary branch of the square roots of λ_1^2 and λ_2^2, depending on whether the radicand is positive or negative, respectively. The solutions for the case $\omega > 0$ then can be found by taking into consideration symmetry relations in the (k_x, ω)-plane: due to the physical nature of the displacements the results in the original domain must be real, i.e. the results for the positive frequencies are the complex conjugates of the results for the negative frequencies and thus exploiting this fact they do not need to be calculated. This is very advantageous because the size of the problem is reduced by half without any further need to distinguish different cases. Finally one arrives at the solution

$$\{\hat{u}\} = [L]\{C\}, \quad \{\hat{\sigma}\} = [T]\{C\} \tag{15}$$

for the displacements

$$\{\hat{u}\}^{\mathrm{T}} = \{\hat{u}_x\, \hat{u}_y\, \hat{u}_z\} \tag{16}$$

and the stresses

$$\{\hat{\sigma}\}^{\mathrm{T}} = \{\hat{\sigma}_x\, \hat{\sigma}_y\, \hat{\sigma}_z\, \hat{\sigma}_{xy}\, \hat{\sigma}_{yz}\, \hat{\sigma}_{zx}\}. \tag{17}$$

The matrices $[L]$ and $[T]$ are given in Appendix A, $\{C\}$ contains the unknown coefficients, which can be evaluated by taking into account the boundary conditions at $z = 0$ and the continuity conditions, if a layered half-space is considered.

As was shown in Refs. [38,39] it is advantageous—if the load moves in x-direction with the velocity v—to use a coordinate system that moves with the same velocity. In the transformed (k_x, ω)-domain then one can apply the results for a locally fixed load, if one substitutes its frequency ω simply by $\bar{\omega} = \omega - vk_x$.

2.2. Solution for a continuum with a cylindrical cavity

Now the solution for the continuum with cylindrical cavity shall be derived. Starting from the Lamé's equation of elastodynamics and after the use of the Helmholtz principle the obtained wave equations can be transformed into cylinder coordinates x, r and ϕ, so one obtains the differential equations for the infinite continuum with cylindrical cavity. In order to arrive at decoupled wave equations starting from Eq. (7), the Christoffel symbols of the respective basis $\mathbf{g}^i$ have to vanish, thus the components Ψ_i of the potentials are referred to a cartesian basis (so that Ψ_y and Ψ_z are used instead of Ψ_r and Ψ_ϕ, although the operators are referred to cylindrical coordinates). Then similarly as for the case of the uniform half-space the component Ψ_x of the vectorial potential Ψ_γ is chosen equal to zero:

$$\left[\frac{\partial^2}{\partial r^2} + \frac{1}{r}\frac{\partial}{\partial r} + \frac{1}{r^2}\frac{\partial^2}{\partial \phi^2} + \frac{\partial^2}{\partial x^2} - \frac{\rho}{\lambda + 2\mu}\frac{\partial^2}{\partial t^2}\right]\Phi = 0, \tag{18}$$

$$\left[\frac{\partial^2}{\partial r^2} + \frac{1}{r}\frac{\partial}{\partial r} + \frac{1}{r^2}\frac{\partial^2}{\partial \phi^2} + \frac{\partial^2}{\partial x^2} - \frac{\rho}{\mu}\frac{\partial^2}{\partial t^2}\right]\Psi_\gamma = 0, \quad \gamma = y, z. \tag{19}$$

As shown in Ref. [40] (the authors are not aware of any publication in English, in which this information can be found), Eqs. (18) and (19) can be decoupled by introducing new functions M_1' and M_2' that combine the potentials Ψ_y and Ψ_z in the following manner:

$$M_1' = \tfrac{1}{2}\mathrm{e}^{\mathrm{i}\phi}(\Psi_y - \mathrm{i}\Psi_z),$$

$$M_2' = \tfrac{1}{2}\mathrm{e}^{-\mathrm{i}\phi}(\Psi_y + \mathrm{i}\Psi_z). \tag{20}$$

In terms of these functions Eqs. (19) take the following form:

$$\left[\frac{\partial^2}{\partial r^2} + \frac{1}{r}\frac{\partial}{\partial r} + \frac{1}{r^2}\left(\frac{\partial^2}{\partial \phi^2} - 2\mathrm{i}\frac{\partial}{\partial \phi} - 1\right) + \frac{\partial^2}{\partial x^2} - \frac{\rho}{\mu}\frac{\partial^2}{\partial t^2}\right]M_1' = 0,$$

$$\left[\frac{\partial^2}{\partial r^2} + \frac{1}{r}\frac{\partial}{\partial r} + \frac{1}{r^2}\left(\frac{\partial^2}{\partial \phi^2} + 2\mathrm{i}\frac{\partial}{\partial \phi} - 1\right) + \frac{\partial^2}{\partial x^2} - \frac{\rho}{\mu}\frac{\partial^2}{\partial t^2}\right]M_2' = 0. \tag{21}$$

For the solution of the problem a series expansion of the potentials Φ, M_1' and M_2' regarding the circumferential direction ϕ is used:

$$\Phi(x, r, \phi) = \sum_{n=-\infty}^{n=\infty} \Phi(x, r, n)\mathrm{e}^{\mathrm{i}n\phi}$$

$$M_1'(x, r, \phi) = \sum_{n=-\infty}^{n=\infty} M_1'(x, r, n)\mathrm{e}^{\mathrm{i}n\phi}$$

$$M_2'(x, r, \phi) = \sum_{n=-\infty}^{n=\infty} M_2'(x, r, n)\mathrm{e}^{\mathrm{i}n\phi}. \tag{22}$$

Together with Eq. (18) and (21) one obtains the following equations for the derivation of the coefficients of the Fourier series:

$$\left[\frac{\partial^2}{\partial r^2}+\frac{1}{r}\frac{\partial}{\partial r}-\frac{n^2}{r^2}+\frac{\partial^2}{\partial x^2}-\frac{1}{c_p^2}\frac{\partial^2}{\partial t^2}\right]\Phi(x,r,n)=0,$$
$$\left[\frac{\partial^2}{\partial r^2}+\frac{1}{r}\frac{\partial}{\partial r}-\frac{(n-1)^2}{r^2}+\frac{\partial^2}{\partial x^2}-\frac{1}{c_s^2}\frac{\partial^2}{\partial t^2}\right]M_1'(x,r,n)=0,$$
$$\left[\frac{\partial^2}{\partial r^2}+\frac{1}{r}\frac{\partial}{\partial r}-\frac{(n+1)^2}{r^2}+\frac{\partial^2}{\partial x^2}-\frac{1}{c_s^2}\frac{\partial^2}{\partial t^2}\right]M_2'(x,r,n)=0. \tag{23}$$

Applying a two-fold Fourier transform with respect to the longitudinal direction and the time ($x\circ\!\!-\!\!\bullet k_x$, $t\circ\!\!-\!\!\bullet\omega$), one arrives at the following equations for the unknown potentials $\hat{\Phi}$, $\hat{M}_1'$ and $\hat{M}_2'$:

$$\left[\frac{\partial^2}{\partial r^2}+\frac{1}{r}\frac{\partial}{\partial r}+\left(-\frac{n^2}{r^2}+\alpha^2k_x^2\right)\right]\hat{\Phi}(k_x,r,n)=0,$$

$$\left[\frac{\partial^2}{\partial r^2}+\frac{1}{r}\frac{\partial}{\partial r}+\left(+\frac{(n-1)^2}{r^2}+\beta^2k_x^2\right)\right]\hat{M}_1'(k_x,r,n)=0,$$

$$\left[\frac{\partial^2}{\partial r^2}+\frac{1}{r}\frac{\partial}{\partial r}+\left(-\frac{(n+1)^2}{r^2}+\beta^2k_x^2\right)\right]\hat{M}_2'(k_x,r,n)=0 \tag{24}$$

with

$$\alpha^2=\frac{(\omega-vk_x)^2}{c_p^2k_x^2}-1 \quad \text{and} \quad \beta^2=\frac{(\omega-vk_x)^2}{c_s^2k_x^2}-1, \tag{25}$$

provided that a moving reference frame is used as described in Section 2.1 for a load moving in x-direction with the velocity v and oscillating with the frequency ω.

The general solution can be written in terms of Bessel functions J_n and Neumann functions Y_n or of Hankel functions of 1st and 2nd kind H_n^1 and H_n^2 instead.

Taking into account the radiation condition of Sommerfeld at $r\to\infty$, one has to arrive at a description for decaying and outgoing waves. Therefore the Bessel functions J_n and the Neumann function Y_n have to be combined in a certain manner. As has been shown in Ref. [35] (the authors are not aware of any publication in English, in which this information can be found) it is favorable to work with the Hankel functions H_n^1, H_n^2

$$\hat{\Phi}(r,n,k_x)=C_{1n}H_n^1(\alpha k_xr)+C_{4n}H_n^2(\alpha k_xr),$$

$$\hat{M}_1'(r,n,k_x)=C_{2n}H_{n-1}^1(\beta k_xr)+C_{5n}H_{n-1}^2(\beta k_xr),$$

$$\hat{M}_2'(r,n,k_x)=C_{3n}H_{n+1}^1(\beta k_xr)+C_{6n}H_{n+1}^2(\beta k_xr) \tag{26}$$

instead of the Bessel functions J_n and the Neumann functions Y_n because then the radiation condition of Sommerfeld can be fulfilled in any case—also in the general case taking into account material damping by the use of complex Lamé's constants—if one chooses as solutions only the Hankel functions of the 1st kind H_n^1 or those of the 2nd kind H_n^2 depending on the sign of the frequency ω: if $\omega<0$ one has to work only with the Hankel functions of the 1st kind H_n^1, if $\omega>0$ one has to construct the solution only using the Hankel functions of the 2nd kind H_n^2. In this context one has to work with the positive real or the positive imaginary branch of the square roots of $\alpha^2k_x^2$ and $\beta^2k_x^2$, depending on whether the radicand is positive or negative, respectively.

As example the potential $\hat{\Phi}$ is given:

$$\hat{\Phi}(r,n,k_x) = \begin{cases} C_{1n}H_n^1(\alpha,k_x,r) & \text{if } \omega<0, \\ C_{4n}H_n^2(\alpha,k_x,r) & \text{if } \omega>0. \end{cases} \tag{27}$$

The solutions for the Potentials $\hat{M}_1'$ and $\hat{M}_2'$ can be found analogously. So by choosing the Hankel functions H_n^1, H_n^2 instead of the Bessel functions J_n and the Neumann functions Y_n as fundamental solution, taking into account the radiation condition reduces the size of the problem by half.

Once the solutions for $\hat{\Phi}$, $\hat{M}_1'$ and $\hat{M}_2'$ are known, one can evaluate—depending on the unknown coefficients $\{C_n\}$—all displacements and stresses $\{S\}$, especially their values at the boundary of the cylindrical cavity, with

$$\{C_n\} = \{C_{1n}\, C_{2n}\, C_{3n}\}^{\mathrm{T}}, \tag{28}$$

$$\{S\} = \left\{ u_r\, u_\phi\, u_x\, \frac{\sigma_{rr}}{2\mu}\, \frac{\sigma_{\phi\phi}}{2\mu}\, \frac{\sigma_{xx}}{2\mu}\, \frac{\sigma_{r\phi}}{2\mu}\, \frac{\sigma_{rx}}{2\mu}\, \frac{\sigma_{\phi x}}{2\mu} \right\}^{\mathrm{T}} \tag{29}$$

in the form

$$\{S\} = [H(r,n,k_x,c,\omega)]\{C_n\}. \tag{30}$$

The three remaining unknowns now can be easily found by accounting for the boundary conditions at the surface of the cylindrical cavity at $r = a$.

For the case of real Lamé's constants $\lambda = \lambda'$ and $\mu = \mu'$ according to Eqs. (2) and (3) the following situations could be distinguished. For $\alpha^2<0, \beta^2<0$ all values of $[H]$ are given in Ref. [40] for the case of a stationary moving load. Those values can be easily adapted to the case of a harmonic oscillating moving load by substituting c by $\bar{c} = v - (\omega/k_x)$. For $\alpha^2>0$ or $\beta^2>0$ or for the general case of complex arguments α and β the matrix $[H]$ takes a similar form, however on the basis of the Hankel functions of the 1st and 2nd kind H_n^1, H_n^2. The values of $[H]$ for this case can be found in Appendix B.

3. Half-space with a cylindrical cavity

For the geometric situation of a half-space with cylindrical cavity it is not possible to find a closed solution. As mentioned before, the solution will be constructed as a superposition of the solutions for the uniform half-space and the continuum with a cylindrical cavity. If a ($x\circ\!\!-\!\!\bullet k_x, t\circ\!\!-\!\!\bullet\omega$) transform is used, it is sufficient to study a plane problem in the (y,z)-plane. Fig. 2 shows that, for given y at the surface of the half-space, one has $\psi = \arctan(y/d)$ and $r = \sqrt{y^2+d^2}$ as respective polar coordinates. In an analogous way for a given r and ψ the respective cartesian coordinates can be found.

With the results given in Section 2.1, it is possible to evaluate (for a given loading at the surface of the half-space) all stresses that act in a uniform half-space, in particular those stresses, that act along the cylindrical

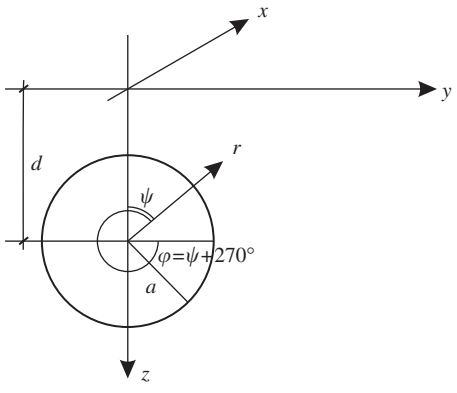

Fig. 2. Coordinate system.

line $r = a$ shown in Fig. 2. In a similar way starting from an infinite continuum with cylindrical cavity, it is possible to evaluate all stresses along the horizontal plane $z = 0$. The stresses on the cylinder should be expressed then in polar coordinates as $\sigma_{rr}, \sigma_{r\phi}, \sigma_{rx}$, whereas the stresses at the plane surface $z = 0$ will be expressed using cartesian coordinates as $\sigma_{zz}, \sigma_{zy}, \sigma_{zx}$. The respective relations are known from elementary mechanics

$$\{\sigma_{rr} \;\; \sigma_{r\phi}\}^{\mathrm{T}} = [T]\{\sigma_{yy} \;\; \sigma_{zz} \;\; \sigma_{zy}\}^{\mathrm{T}} \tag{31}$$

with

$$[T] = \begin{bmatrix} \sin^2\phi & \cos^2\phi & 2\sin\phi\cos\phi \\ -\cos\phi\sin\phi & \cos\phi\sin\phi & \sin^2\phi - \cos^2\phi \end{bmatrix}. \tag{32}$$

Additionally to the well-known relations at $r = a$ for a plane state of stress one has

$$\sigma_{rx} = -\sigma_{zx}\cos\psi + \sigma_{yx}\sin\psi \tag{33}$$

for the stresses in the longitudinal direction x.

Similar relations hold for the ''cartesian'' stresses at $z = 0$ depending on the stresses $\sigma_{rr}, \sigma_{r\phi}, \sigma_{rx}$.

In order to observe the boundary conditions both at the surface of the cylindrical cavity and at the plane surface $z = 0$, unknown stress states according to polar coordinates $[\sigma_n^{(h)}]$ will be applied at the cylindrical cavity and unknown stress states according to cartesian coordinates $[\sigma_m^{(s)}]$ at the surface $z = 0$. The indices n and m refer to the number of the Fourier series expansion at the cylindrical surface Γ_s and to the members of the numerical Fourier transform at the surface $z = 0$, respectively.

One possibility to observe those boundary conditions would be an iteration procedure, but the chosen more elegant approach allows a closed solution: each Fourier series member on the cylindrical surface at $r = a$ causes stresses at the surface $z = 0$ and vice versa. Now at the surface of the half-space not only the stresses applied there $[\sigma_m^{(s)}]$ but also the stresses $[\sigma_{mn}^{(sh)}]$, which arise due to the stresses acting at the surface of the cylindrical cavity, are described by the coefficients of their numerical Fourier integrals. In an analogous procedure all stresses acting at the cylindrical cavity are expanded into a Fourier series, not only the stresses due to the stresses applied at the cavity $[\sigma_n^{(h)}]$ but also the stresses $[\sigma_{nm}^{(hs)}]$, which arise at the surface of the cylindrical cavity due to the stresses acting at the surface of the half-space. If at the surface of the cavity a stress state $[\sigma_n^{(p)}]$ due to a given external load exists, one can evaluate all the coefficients of the unknown stress states taking into consideration the condition, that at the surface of the half-space all stresses have to vanish while at the surface of the cylindrical cavity the given external load $[\sigma_n^{(p)}]$ is obtained. This condition must be fulfilled for all wavenumbers k_y of the numerical Fourier integrals at the surface of the half-space as well as for all Fourier series members at the surface of the cavity. Finally, a closed solution can be found by solving one compound system of $3m + 3n + 4$ (in the case the loading is symmetric with respect to the vertical z-axis; the general case of an arbitrary loading can be obtained by a superposition of the symmetric and the antimetric load case) linear equations for all stress coefficients $[C_{(s)}^m]$ and $[C_{(h)}^n]$:

$$\begin{bmatrix} [\sigma_m^{(s)}] & [\sigma_{mn}^{(sh)}] \\ [\sigma_{nm}^{(hs)}] & [\sigma_n^{(h)}] \end{bmatrix} \begin{bmatrix} [C_{(s)}^m] \\ [C_{(h)}^n] \end{bmatrix} = \begin{bmatrix} [0] \\ [\sigma_n^{(p)}] \end{bmatrix}. \tag{34}$$

The accuracy is restricted by the number of series members taken into account.

Once the unknowns are evaluated one can calculate also all displacements, e.g. those on the surface of the cylindrical cavity Γ_s. With these quantities a matrix $\mathbf{N}^{\infty}$ can be derived for each k_x, ω that describes the response characteristics on the cylindrical cavity of a half-space by the variation of the work of the stresses along the cylindrical surface Γ_s. As mentioned before in order to exploit the invariant cross-section of the system in the longitudinal direction x, all functions are given by their Fourier transform with respect to their variability in longitudinal direction. As shown in Ref. [41], in this case the complete volume integral needed to derive the matrix $\mathbf{N}^{\infty}$ for the half-space with a cylindrical cavity can be reduced to an integral over the area in

the (y,z)-plane and an additional integral over the wavenumbers k_x by the use of the Parseval's theorem:

$$\begin{aligned}\int_{-\infty}^{+\infty}\delta\mathbf{u}(x)\mathbf{t}(x)\,\mathrm{d}x &= \int_{-\infty}^{+\infty}\delta\mathbf{u}(x)\left[\frac{1}{2\pi}\int_{-\infty}^{+\infty}\hat{\mathbf{t}}(k_x)\mathrm{e}^{\mathrm{i}k_x x}\,\mathrm{d}k_x\right]\mathrm{d}x\\ &= \frac{1}{2\pi}\int_{-\infty}^{+\infty}\left[\int_{-\infty}^{+\infty}\delta\mathbf{u}(x)\mathrm{e}^{\mathrm{i}k_x x}\,\mathrm{d}x\right]\hat{\mathbf{t}}(k_x)\,\mathrm{d}k_x\\ &= \frac{1}{2\pi}\int_{-\infty}^{+\infty}\left[\int_{-\infty}^{+\infty}\delta\mathbf{u}(x)\mathrm{e}^{-\mathrm{i}(-k_x)x}\,\mathrm{d}x\right]\hat{\mathbf{t}}(k_x)\mathrm{d}k_x\\ &= \frac{1}{2\pi}\int_{-\infty}^{+\infty}\delta\hat{\mathbf{u}}(-k_x)\hat{\mathbf{t}}(k_x)\mathrm{d}k_x = \frac{1}{2\pi}\int_{-\infty}^{+\infty}\delta\hat{\mathbf{u}}(k_x)\hat{\mathbf{t}}(-k_x)\,\mathrm{d}k_x.\end{aligned} \tag{35}$$

Finally, one obtains the matrix $\mathbf{N}^{\infty}$ characterizing the force–displacement behavior at the cylindrical surface Γ_s of the half-space with cylindrical cavity with respect to the coefficients of the Fourier series representation of the stresses at the surface Γ_s:

$$\begin{aligned}\delta U_{\infty}(k_x) &= \int_{\Gamma}\delta\mathbf{u}(-k_x)\mathbf{t}(k_x)\mathrm{d}\Gamma\\ &= \int_{\Gamma}\delta C^k(-k_x)\frac{\partial\mathbf{u}(-k_x)}{\partial C^k(-k_x)}\frac{\partial\mathbf{t}(k_x)}{\partial C^l(k_x)}C^l(k_x)\mathrm{d}\Gamma\\ &= \delta C^k(-k_x)\int_{\Gamma}u_k(-k_x)\delta t_l(k_x)\mathrm{d}\Gamma C^l(k_x)\\ &=:\delta C^k(-k_x)N^{\infty}_{kl}C^l(k_x).\end{aligned} \tag{36}$$

4. Finite element description for a tunnel with an arbitrary, non circular cylindrical shape

Between stress and strain the following relation depending on the Lamé's constants λ and μ holds:

$$\sigma^{ij} = 2\mu\varepsilon^{ij} + \lambda\varepsilon^m_m g^{ij}. \tag{37}$$

The strains ε_{ij} are given with respect to the displacements u_i:

$$\varepsilon_{ij} = \tfrac{1}{2}[u_i|_j + u_j|_i], \quad i,j = \{x,y,z\}. \tag{38}$$

Applying a Fourier transform with respect to the longitudinal direction ($x\circ\!\!-\!\!\bullet k_x$) yields:

$$\hat{\boldsymbol{\varepsilon}} = \begin{Bmatrix}\mathrm{i}k_x\hat{u}\\ \hat{v}_{,y}\\ \hat{w}_{,z}\\ \hat{u}_{,y}+\mathrm{i}k_x\hat{v}\\ \hat{v}_{,z}+\hat{w}_{,y}\\ \mathrm{i}k_x\hat{w}+\hat{u}_{,z}\end{Bmatrix} = \hat{\mathbf{G}}\hat{\mathbf{u}} = \begin{bmatrix}\mathrm{i}k_x & 0 & 0\\ 0 & \frac{\partial}{\partial y} & 0\\ 0 & 0 & \frac{\partial}{\partial z}\\ \frac{\partial}{\partial y} & \mathrm{i}k_x & 0\\ 0 & \frac{\partial}{\partial z} & \frac{\partial}{\partial y}\\ \frac{\partial}{\partial z} & 0 & \mathrm{i}k_x\end{bmatrix}\begin{Bmatrix}\hat{u}\\ \hat{v}\\ \hat{w}\end{Bmatrix}. \tag{39}$$

In the following, the stiffness matrix is derived by the use of the principle of virtual work. One obtains the virtual work by the inner stresses δW_i, the virtual work of the inertia forces δW_T and the virtual work done by the external forces δW_a:

$$\delta W_i = -\int\delta\boldsymbol{\varepsilon}^{\mathrm{T}}\boldsymbol{\sigma}\,\mathrm{d}V = -\int\delta\boldsymbol{\varepsilon}^{\mathrm{T}}\mathbf{D}\boldsymbol{\varepsilon}\,\mathrm{d}V,$$

$$\delta W_T = -\int \delta \mathbf{u}^{\mathrm{T}} \rho \ddot{\mathbf{u}} \, \mathrm{d}V,$$

$$\delta W_a = \int \delta \mathbf{u}^{\mathrm{T}} \mathbf{p} \, \mathrm{d}A. \tag{40}$$

For a tunnel with an arbitrary, non-circular cross-sectional shape it does not make sense to use polar coordinates for the description of its stress state. In this case a FE description shall be applied for the tunnel structure itself and a certain portion of its surrounding. In order to keep the computational effort low, the FEM calculation will be applied in a (k_x, y, z, ω)-domain, so the discretization can follow usual 2D discretization techniques in the (y, z)-plane. The Finite Element calculation must be executed not only for every frequency ω, but also for every wavenumber k_x. The respective equations are derived then—as shown in Ref. [34]—by again applying the Parseval's theorem, which allows to derive the stiffness matrix of the respective FEM description in the transformed domain and thus reduces the integral over the volume to a basic 2D integral over the discretized (y, z)-plane.

Here the Parseval's theorem is applied to the strains $\delta\boldsymbol{\varepsilon}(x)$ and the stresses $\boldsymbol{\sigma}(x)$ in an analogous way as shown by Eq. (35). Now the virtual work by the inner stresses and the virtual work by the inertia forces can be formulated by the use of the well known abbreviations **B** and **N**:

$$\delta W_i = -\int_{-\infty}^{+\infty} \left[\delta \mathbf{u}^{\mathrm{T}}(-k_x) \int_z \left[\int_y \mathbf{B}^{\mathrm{T}}(-k_x) \mathbf{D} \mathbf{B}(k_x) \, \mathrm{d}y \right] \mathrm{d}z \, \mathbf{u}(k_x) \right] \mathrm{d}k_x,$$

$$\delta W_T = \int_{-\infty}^{+\infty} \omega^2 \left[\delta \mathbf{u}^{\mathrm{T}}(-k_x) \int_z \left[\int_y \mathbf{N}^{\mathrm{T}} \rho \mathbf{N} \, \mathrm{d}y \right] \mathrm{d}z \, \mathbf{u}(k_x) \right] \mathrm{d}k_x. \tag{41}$$

As was discussed in Ref. [32] (the authors are not aware of any publication in English, in which this information can be found) it is advantageous (in regard of the numerical performance) to use as FEM unknowns the coefficients of the Fourier series representation of the solution at the surface of the cylindrical cavity. This corresponds to a change of basis

$$\{u_\Gamma\} = [A]\{C_j^h\}. \tag{42}$$

Here $\{u_\Gamma\}$ are the FEM dofs at the contact points with the half-space. With this relation the virtual work yields:

$$\delta W_i = -\int_{-\infty}^{+\infty} \left[\delta \mathbf{C}_n^{\mathrm{T}}(-k_x) \mathbf{A}^{\mathrm{T}}(-k_x) \int_z \left[\int_y \mathbf{B}^{\mathrm{T}}(-k_x) \mathbf{D} \mathbf{B}(k_x) \, \mathrm{d}y \right] \mathrm{d}z \mathbf{A}(k_x) \mathbf{C}_n(k_x) \right] \mathrm{d}k_x,$$

$$\delta W_T = \int_{-\infty}^{+\infty} \omega^2 \left[\delta \mathbf{C}_n^{\mathrm{T}}(-k_x) \mathbf{A}^{\mathrm{T}}(-k_x) \int_z \left[\int_y \mathbf{N}^{\mathrm{T}} \rho \mathbf{N} \, \mathrm{d}y \right] \mathrm{d}z \mathbf{A}(k_x) \mathbf{C}_n(k_x) \right] \mathrm{d}k_x. \tag{43}$$

The dynamic equilibrium is fulfilled if the sum of the virtual work vanishes:

$$\delta W = \delta W_i + \delta W_T + \delta W_a = 0, \tag{44}$$

$$\delta W = \int_{-\infty}^{+\infty} \delta \mathbf{C}_n^{\mathrm{T}}(-k_x) \mathbf{A}^{\mathrm{T}}(-k_x) \Bigg(\Bigg[-\int_z \int_y \mathbf{B}^{\mathrm{T}}(-k_x) \mathbf{D} \mathbf{B}(k_x) \, \mathrm{d}y \, \mathrm{d}z + \omega^2 \int_y \int_z \mathbf{N}^{\mathrm{T}} \rho \mathbf{N} \, \mathrm{d}y \, \mathrm{d}z \Bigg] \mathbf{A}(k_x) \mathbf{C}_n(k_x) + \int_s \mathbf{N}^{\mathrm{T}} \mathbf{p}(k_x) \, \mathrm{d}s \Bigg) \mathrm{d}k_x = 0. \tag{45}$$

Taking into consideration that the virtual displacement field $\delta \mathbf{u}_0^{\mathrm{T}}(-k_x)$ is arbitrary and non-zero

$$\delta \mathbf{u}^{\mathrm{T}}(-k_x) \text{ arbitrary}, \neq 0, \tag{46}$$

it can be eliminated from the condition. Finally, one obtains the given equilibrium equation:

$$\left(-\underbrace{\int_z \int_y \mathbf{B}^{\mathrm{T}}(-k_x)\mathbf{D}\mathbf{B}(k_x)\,\mathrm{d}y\,\mathrm{d}z}_{\tilde{K}} + \omega^2 \underbrace{\int_y \int_z \mathbf{N}^{\mathrm{T}}\rho\mathbf{N}\,\mathrm{d}y\,\mathrm{d}z}_{\tilde{M}} \right) \mathbf{u}_0(k_x) + \mathbf{p}_0(k_x) = 0. \tag{47}$$

This equation can be written by the use of the given abbreviations as a classical Finite Element equation:

$$[\mathbf{K} - \omega^2\mathbf{M}]\mathbf{u}_0(k_x) = \mathbf{p}_0(k_x), \tag{48}$$

$$\mathbf{K}_{dyn}\mathbf{u}_0(k_x) = \mathbf{p}_0(k_x). \tag{49}$$

If the stiffness matrix of the FEM domain Ω is partitioned according to

$$\begin{Bmatrix} \mathbf{F}_\Omega \\ \mathbf{F}_\Gamma \end{Bmatrix} = \begin{bmatrix} \mathbf{K}_{11} & \mathbf{K}_{12} \\ \mathbf{K}_{21} & \mathbf{K}_{22} \end{bmatrix} \begin{Bmatrix} \mathbf{u}_\Omega \\ \mathbf{u}_\Gamma \end{Bmatrix}, \tag{50}$$

where $\mathbf{u}_\Omega$ are the FEM dofs except those at the contact points, then with the matrix $\mathbf{N}^\infty$ of the soil as given by Eq. (36) the basic modified FEM equations can be written as

$$\begin{bmatrix} \mathbf{K}_{11} & \mathbf{K}_{12}\mathbf{A} \\ \mathbf{A}^{\mathrm{T}}\mathbf{K}_{21} & \mathbf{N}^\infty + \mathbf{A}^{\mathrm{T}}\mathbf{K}_{22}\mathbf{A} \end{bmatrix} \begin{Bmatrix} \mathbf{u}_\Omega \\ \mathbf{C}_{\mathbf{j}}^{\mathbf{h}} \end{Bmatrix} = \begin{Bmatrix} \mathbf{F}_\Omega \\ 0 \end{Bmatrix}. \tag{51}$$

5. Interaction of a mass–spring system with a nonlinear sdof system

Having derived the solution for the system *half-space–tunnel–structure*, the interaction of a mass–spring system with a nonlinear sdof system shall be described. As shown in Fig. 3 the elastic support is mounted on the tunnel shell which itself is coupled to the half-space. Once the displacements of the footings of the support elements are known in relation to the applied forces at the center of the footings one can derive by inversion a respective dynamic *stiffness* k_{cs}, which depends on the wavenumber k_x and the frequency ω. The term *stiffness* was in this context introduced by Dietermann and Metrikine [42] for the case of a half-space. The plate which is assumed as rigid in transversal direction and thus modelled as a beam, reduces in the transformed domain to a mass on an elastic support, which has two parallel contributions—the bending stiffness of the plate and an elastic foundation. The elastic foundation itself is a series system of the elastic support elements k_w (with an inclination γ with respect to the vertical axis) and the stiffness of its footing k_{cs} (Fig. 3).

$$\frac{1}{k} = \frac{1}{k_w} + \frac{1}{k_{cs}} = \frac{k_{cs} + k_w}{k_w k_{cs}}. \tag{52}$$

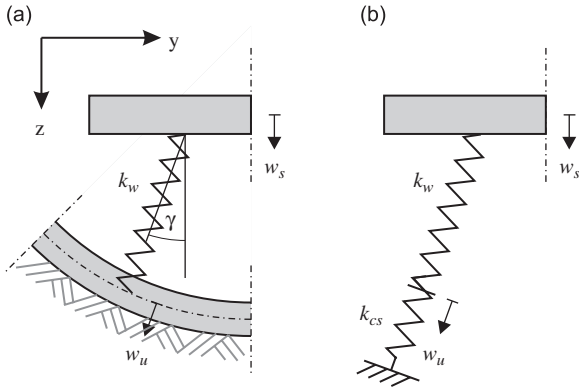

Fig. 3. Tunnel with mass–spring system: real system (a) and idealized system (b).

The displacement of the beam now can be calculated as the quotient of the load $\tilde{p}(k_x,\omega)$ and a "stiffness" $\tilde{D}(k_x,\omega)$:

$$\tilde{w}(k_x,\omega)=\frac{\tilde{p}(k_x,\omega)}{K(k_x,\omega)-m\omega^2}=\frac{\tilde{p}(k_x,\omega)}{\tilde{D}(k_x,\omega)}. \tag{53}$$

The "stiffness" $\tilde{D}(k_x,\omega)$ is given depending on the frequency ω and the wavenumber k_x and represents the complete coupled system *beam–tunnel–soil*.

$$\tilde{D}(k_x,\omega)=k_x^4 EI_{pl}+\frac{k_w k_{cs}}{k_w+k_{cs}}\cos^2\gamma-m\omega^2. \tag{54}$$

Now the derivation of the response of the coupled system due to a moving time depending load $p(x,t)=P(t)\delta(x-vt)$ shall be shown. In the case of the interaction problem under consideration this load is the interaction force that is given here in the Fourier transformed domain.

$$\tilde{p}(k_x,\omega)=\tilde{P}(\omega+vk_x). \tag{55}$$

After a 2D IFT ($k_x\bullet\!\!-\!\!\circ x,\ \omega\bullet\!\!-\!\!\circ t$) one obtains the displacement of the beam in the moving coordinate system at $x=vt$:

$$\begin{aligned} w(x=vt,t)&=\frac{1}{4\pi^2}\int_{-\infty}^{\infty}\int_{-\infty}^{\infty}\frac{\tilde{p}(k_x,\omega)}{\tilde{D}(k_x,\omega)}\mathrm{e}^{\mathrm{i}k_x vt}\mathrm{e}^{\mathrm{i}\omega t}\,\mathrm{d}k_x\,\mathrm{d}\omega\\ &=\frac{1}{4\pi^2}\int_{-\infty}^{\infty}\int_{-\infty}^{\infty}\frac{\tilde{P}(\omega+vk_x)}{\tilde{D}(k_x,\omega)}\mathrm{e}^{\mathrm{i}(\omega+vk_x)t}\,\mathrm{d}k_x\,\mathrm{d}\omega. \end{aligned} \tag{56}$$

Introducing the substitution $\omega'=\omega+vk_x$ this equation yields:

$$w(x=vt,t)=\frac{1}{4\pi^2}\int_{-\infty}^{\infty}\int_{-\infty}^{\infty}\frac{\tilde{P}(\omega')}{\tilde{D}(k_x,\omega'-vk_x)}\,\mathrm{d}k_x\mathrm{e}^{\mathrm{i}\omega' t}\,\mathrm{d}\omega'. \tag{57}$$

If one introduces the system transfer function

$$\tilde{H}(\omega')=\frac{1}{2\pi}\int_{-\infty}^{\infty}\frac{1}{\tilde{D}(k_x,\omega'-vk_x)}\,\mathrm{d}k_x, \tag{58}$$

this expression equals to the IFT of the product of the interaction force $\tilde{P}(\omega')$ and the system transfer function $\tilde{H}(\omega')$:

$$w_B(t)=w(x=vt,t)=\frac{1}{2\pi}\int_{-\infty}^{\infty}(\tilde{P}(\omega')\tilde{H}(\omega'))\mathrm{e}^{\mathrm{i}\omega' t}\,\mathrm{d}\omega'=\mathrm{IFT}(\tilde{P}(\omega')\tilde{H}(\omega')). \tag{59}$$

This product in the transformed domain corresponds to a convolution in the original time domain of the loading $p(t)$ with the impulse response function $h(t)$ that can be obtained as the IFT of the system transfer function.

$$h(t)=\frac{1}{2\pi}\int_{-\infty}^{\infty}\tilde{H}(\omega')\mathrm{e}^{\mathrm{i}\omega' t}\mathrm{d}\omega'. \tag{60}$$

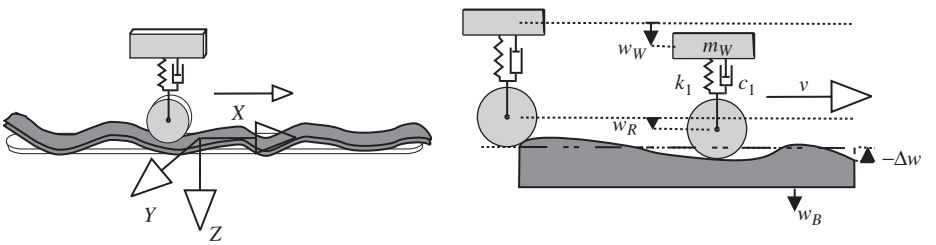

Fig. 4. Modelling the vehicle as sdof system with rail surface unevenness $\Delta w(x)$.

This impulse response function represents completely the behavior of the coupled system consisting of the mass–spring system, the tunnel structure and the half-space. With that, the displacements of the plate may be expressed as a Duhamel integral

$$w_B(t) = \int_0^t P(\tau)h(t-\tau)\,\mathrm{d}\tau. \tag{61}$$

Fig. 4 shows the geometrical situation for a sdof system. The interaction between the complete system and the sdof system is excited by a rail surface unevenness $\Delta w(x)$ as shown in the figure. If the response is described in a moving coordinate system, only the point $\bar{x} = x - vt = 0$ has to be considered. The unevenness causes that the displacement of the footing of the sdof system differs from the displacement of the plate w_B.

The equation of motion of the sdof system with a nonlinear restoring force $F_k(w_W - w_R)$ due to a nonlinear characteristic of the spring $k_1(w_W - w_R)$ and a linear damping force $F_c(\dot{w}_W - \dot{w}_R)$ has the following form:

$$m_W\ddot{w}_W + c_1(\dot{w}_W - \dot{w}_R) + k_1(w_W - w_R) = 0. \tag{62}$$

As shown in Fig. 4, the footing displacement of the sdof system results from the unevenness $\Delta w(t)$ and the displacement of the beam $w_B(t)$ which depends on the history of the interaction force.

$$w_R(t) = w_B(t) - \Delta w(t) = \int_0^t P(\tau)h(t-\tau)\,\mathrm{d}\tau - \Delta w(t). \tag{63}$$

The missing equation can be found from the equation of the vertical dynamic equilibrium for the whole nonlinear sdof system.

$$P(t) = -m_W\ddot{w}_W = c_1(\dot{w}_W - \dot{w}_R) + k_1(w_W - w_R). \tag{64}$$

Those three equations constitute a system of two differential equations and one equation which contains an integral, but no derivatives for the three unknowns w_W, w_B and $P(t)$. Such a system is called a system of "retarding differential algebraic equations" (RDAE) [43] (the authors are not aware of any publication in English, in which this information can be found).

RDAE is a class of equations with special, unfavorable numerical properties. Numerical procedures, even using well established integration schemes as e.g. the Newmark-β method, may lead here to instabilities or significant erroneous high-frequency effects. These effects have purely numerical origin, i.e. the frequencies are reciprocally proportional to the time step. Unfortunately, those high-frequency contributions cannot be removed by choosing smaller time steps. Because it is not possible to go into detail here, it will only be mentioned that the behavior of the system depends decisively on the so-called system index, which counts the number or differentiations to be applied to an algebraic or as in this case retarding equation in order to achieve a pure system of differential equations [43].

For the numerical solution of the given system of nonlinear RDAE for three unknowns there exist two possibilities: the problem can be solved with or without elimination of the interaction force $P(t)$. First the procedure by elimination of the interaction force shall be shown. The numerical representation of the convolution integral can be written as

$$w_R(t) = \int_0^t P(\tau)h(t-\tau)\,\mathrm{d}\tau - \Delta w(t) \rightarrow w_R^{i+1} = w^{\mathrm{hist}} + \frac{\Delta t}{4}P^{i+1}(h^0 + h^1) - \Delta w^{i+1} \tag{65}$$

with the "historical contributions" of $P(t)$ from earlier steps

$$w^{\mathrm{hist}} = \frac{\Delta t}{4}\sum_{k=1}^{i} P^k(h^{\mathrm{i}+1-k+1} + 2h^{\mathrm{i}+1-k} + h^{\mathrm{i}+1-k-1}) - \Delta w^{i+1}. \tag{66}$$

This equation easily can be solved for the interaction force $P(t)$:

$$P^{i+1} = \frac{w_R^{i+1} + \Delta w^{i+1} - w^{\mathrm{hist}}}{\Delta t/4(h^0 + h^1)}. \tag{67}$$

Now the interaction force $P(t)$ can be eliminated out of the system of equations. Finally, one obtains a system consisting just of differential equations, therefore the problems of RDAE will not occur.

Due to the fact that the elimination of the interaction force enforces prior analytical operations, in most cases particularly with regard to the numerical implementation it is preferable not to eliminate the interaction force. Then it is essential to reduce the before mentioned RDAE system index. For the system under consideration this can be achieved by a differentiation of the wheel displacement $w_R(t)$ given by Eq. (63) with respect to the time t:

$$\dot{w}_R(t) = \int_0^t P(\tau)\dot{h}(t-\tau)\,\mathrm{d}\tau - \Delta\dot{w}(t). \tag{68}$$

In the frequency domain this corresponds to a multiplication of the system transfer function $\tilde{H}(\omega')$ by $\mathrm{i}\omega'$:

$$\dot{h}(t) = \frac{1}{2\pi}\int_{-\infty}^{\infty} \mathrm{i}\omega'\tilde{H}(\omega')\mathrm{e}^{\mathrm{i}\omega' t}\,\mathrm{d}\omega'. \tag{69}$$

However, after this multiplication the function that has to be subjected to the IFT does no longer decrease sufficiently quickly, it attenuates only slowly with increasing circular frequency ω. Accordingly, the velocity

$$\dot{w}_B(t) = \int_0^t P(t)\dot{h}(t-\tau)\,\mathrm{d}\tau + P(t)h(0) \tag{70}$$

shows a singular value at the time $t = 0$. The reason for this is the only gradually increasing activated mass of the *beam–tunnel–soil* system.

In order to overcome the problem of the determination of the "singular part" contribution the following relations can be used:

$$\begin{aligned}\frac{1}{2\pi}\int_{-\infty}^{\infty}\dot{h}(t)\,\mathrm{d}t &= \frac{1}{2\pi}\int_{-\infty}^{\infty}\dot{h}(t)\mathrm{e}^{\mathrm{i}0t}\,\mathrm{d}t \\ &= \mathrm{IFT}(\dot{h}(t))|_{\omega'=0} = \mathrm{i}\omega'\tilde{H}(\omega')|_{\omega'=0} = 0,\end{aligned} \tag{71}$$

which result in

$$\int_{-\infty}^{\infty}\dot{h}(t)\,\mathrm{d}t = 0. \tag{72}$$

Observing causality one obtains:

$$\int_{-\infty}^{\infty}\dot{h}(t)\,\mathrm{d}t = \int_{-\infty}^{\Delta t}\dot{h}(t)\,\mathrm{d}t + \int_{\Delta t}^{\infty}\dot{h}(t)\,\mathrm{d}t = \int_{0}^{\Delta t}\dot{h}(t)\,\mathrm{d}t + \int_{\Delta t}^{\infty}\dot{h}(t)\,\mathrm{d}t = 0. \tag{73}$$

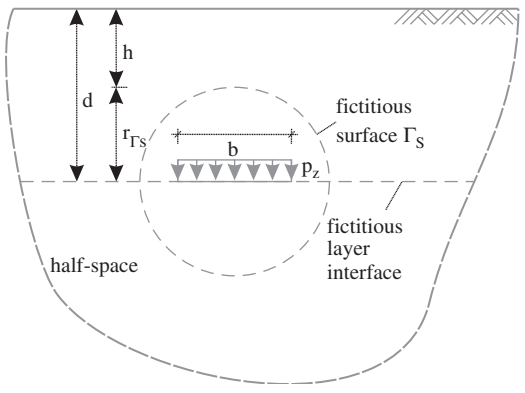

Fig. 5. Half-space with fictitious layer interface and fictitious surface Γ_s.

Taking into account that the impulse response functions $h(t) \to 0$ for $t \to \infty$, the singular part contribution can be calculated.

$$\int_0^{\Delta t} \dot{h}(t)\,\mathrm{d}t = -\int_{\Delta t}^{\infty} \dot{h}(t)\,\mathrm{d}t = -h(\infty) + h(\Delta t) = h(\Delta t)$$
$$= \mathrm{IFT}(\tilde{H}(\omega'))|_{t=\Delta t} = \frac{1}{2\pi}\int_{-\infty}^{\infty} \tilde{H}(\omega')\mathrm{e}^{\mathrm{i}\omega'\Delta t}\,\mathrm{d}\omega'. \tag{74}$$

One obtains this contribution as the IFT of the system transfer function $\tilde{H}(\omega')$ evaluated at the time $t = \Delta t$, which can be used since the interaction force $P(t)$ is considered as constant within each time step. Now a nonlinear procedure as e.g. the Newmark-β method can be applied.

6. Examples

In order to control the functional capability of the presented solution a special situation shall be investigated which is characterized by its property that it can be solved not only by the presented ITM–FEM coupling, but also by a simple semi-analytical approach. As shown in Fig. 5 one soil layer with thickness d resting on a half-space—both modelled with the same soil parameters—with a loading p_z (width b) applied at the interface between the upper layer and the half-space is modelled by the ITM. This situation can also be solved by the method presented here if the complete FEM domain interior of the fictitious surface Γ_s is described by the aid of Finite Elements to which the same material parameters are assigned as to the adjacent soil. Nodes have to be defined along the fictitious surface Γ_s as well as along the fictitious interface between the upper layer and the half-space where the loading p_z shall be applied.

Fig. 6 shows the results for the displacements at the surface of the half-space due to a rectangular loading $p_z = 0.5\,\mathrm{MN/m^2}$ with the width $b = 5\,\mathrm{m}$ in transversal and the length $l = 5\,\mathrm{m}$ in longitudinal direction,

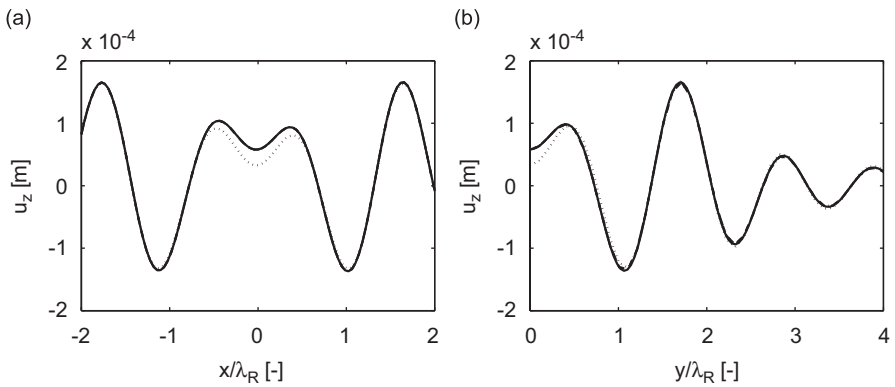

Fig. 6. Displacements at the surface of the half-space; semi-analytical solution for a load acting at the layer interface in the half-space (–) and the ITM–FEM solutions taking into account $n = 3$ (···), $n = 6$ (- -) and $n = 9$ (-·) Fourier series members in circumferential direction, respectively ($f = 50\,\mathrm{Hz}, h = 10\,\mathrm{m}$); the x-axis shows the coordinates x and y, respectively, relative to the wavelength of the Rayleigh wave λ_R: (a) $t = 0$; (b) $t = 0$.

Table 1
Parameters for the soil

Young's modulus E ($\mathrm{Nm^{-2}}$)	Poisson's ratio ν dimensionless	Density ρ ($\mathrm{kg/m^3}$)	Loss factor ζ dimensionless	P-wave speed v_s (m/s)	S-wave speed v_p (m/s)
2000×10^6	0.3	2000	0.10	1160	620

moving with the velocity $v = 20\,\mathrm{m/s}$ and harmonically oscillating with the frequency $f = 50\,\mathrm{Hz}$. The FEM-mesh has been created using triangular elements, for the soil the parameters given in Table 1 have been used. It can be seen that the agreement between the analytical and the FEM solution is very good even if a low number of Fourier series members in circumferential direction is taken into account.

The presented approach allows to calculate the vibrations at the surface of the half-space due to a train moving in a tunnel. Since an ITM–FEM coupling is used, it is possible to model tunnels which may have an

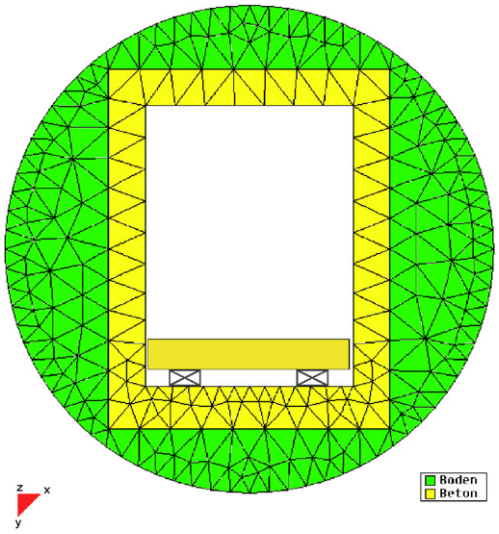

Fig. 7. Finite element mesh for a tunnel with rectangular cross-section and mass–spring system.

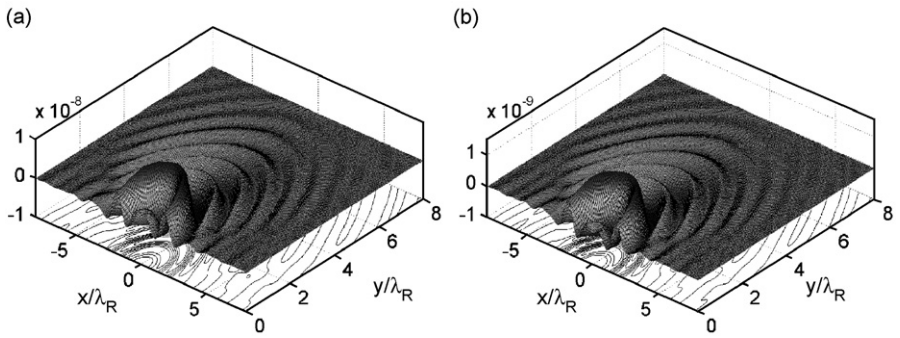

Fig. 8. Vibrations at the surface of the half-space, tunnel with rectangular cross section ($t = 0$): (a) unisolated; (b) isolated ($f_0 = 16\,\mathrm{Hz}$).

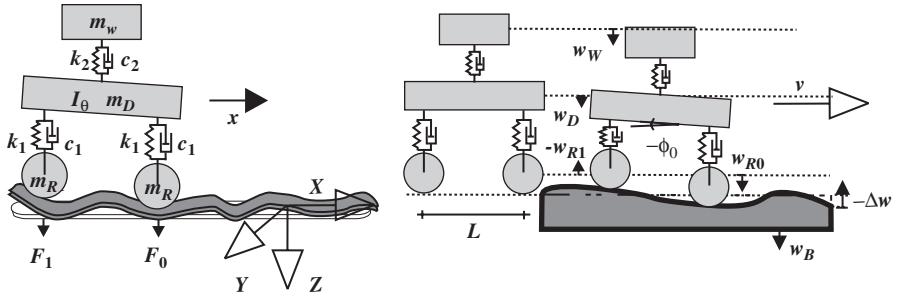

Fig. 9. Modelling the vehicle as bogie system with rail surface unevenness $\Delta w(x)$.

arbitrary cross-sectional shape (Fig. 7). The given mass–spring system will be modelled analytically as described in Section 5.

Fig. 8 shows the displacements at the surface of the half-space due to a load with the amplitude $F_0 = 2 \times 10^3$ N moving in the tunnel with the velocity $v = 20$ m/s. The load is harmonically oscillating

Table 2
Parameters for the vehicle

Distance between axles, m	Δl	2.5
Railcar body mass, kg	m_W	20300
Bogie mass, kg	m_D	2980
Wheelset mass, kg	m_R	1760
Stiffness primary suspension (basic value), N/m	k_0	7.04×10^5
Damping ratio primary suspension, Ns/m	c_1	2.02×10^4
Stiffness secondary suspension, N/m	k_2	19.44×10^5
Damping ratio secondary suspension, Ns/m	c_2	2.38×10^4
Bogie moment of inertia, kg m^2	I_θ	650
Amplitude of the out-of-roundnesses, m	A	1.5×10^{-5}

Table 3
Parameters for the tunnel shell

Young's modulus E (Nm^{-2})	Poisson's ratio ν dimensionless	Density ρ (kg/m^3)	Loss factor ζ dimensionless	Inner radius r_i (m)	Outer radius r_o (m)
30000×10^6	0.2	2500	0	3.0	3.15

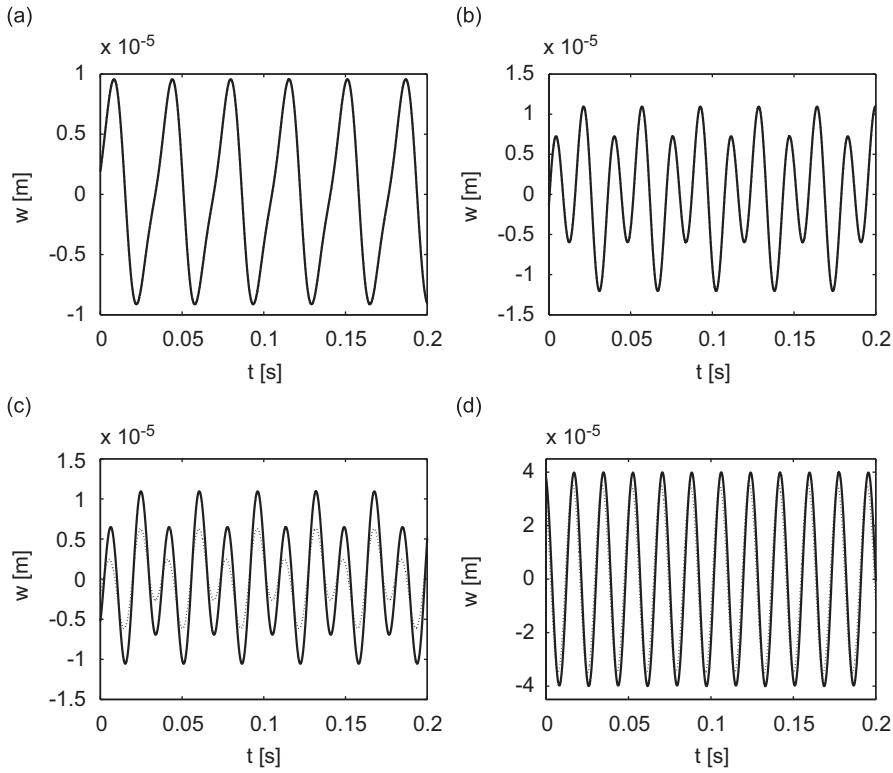

Fig. 10. Wheel displacements w_{R0} ($f_{R0} = 28$) and w_{R1} ($f_{R1} = 56$ Hz) due to wheel out-of-roundnesses with the amplitude $A = 1.5\text{e}{-5}\,m$ for the case of the floating slab-track coupled to the tunnel shell embedded in the half-space (–) and for the case of the floating slab-track on a rigid foundation (···). (a) w_{R0} ($f_0 = 10$ Hz); (b) w_{R1} ($f_0 = 10$ Hz); (c) w_{R0} ($f_0 = 100$ Hz); (d) w_{R1} ($f_0 = 100$ Hz).

with the frequency $f = 50\,\text{Hz}$. The displacements are shown at the time $t = 0$ for the unisolated case and for the case that the tunnel is equipped with a mass–spring system with the natural frequency $f_0 = 16\,\text{Hz}$.

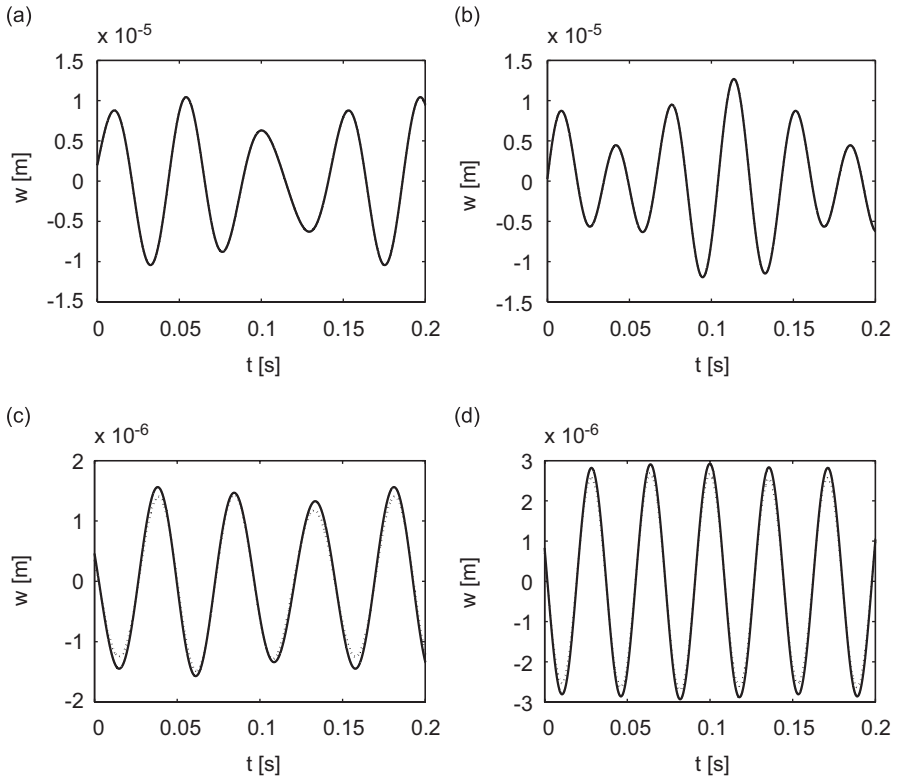

Fig. 11. Wheel displacements $w_{R0}(f_{R0} = 21\,\text{Hz})$ and $w_{R1}(f_{R1} = 28\,\text{Hz})$ due to wheel out-of-roundnesses with the amplitude $A = 1.5\text{e}{-5}\,m$ for the case of the floating slab-track coupled to the tunnel shell embedded in the half-space (–) and for the case of the floating slab-track on a rigid foundation $(\cdots)$. (a) w_{R0} $(f_0 = 10\,\text{Hz})$; (b) w_{R1} $(f_0 = 10\,\text{Hz})$; (c) w_{R0} $(f_0 = 100\,\text{Hz})$; (d) w_{R1} $(f_0 = 100\,\text{Hz})$.

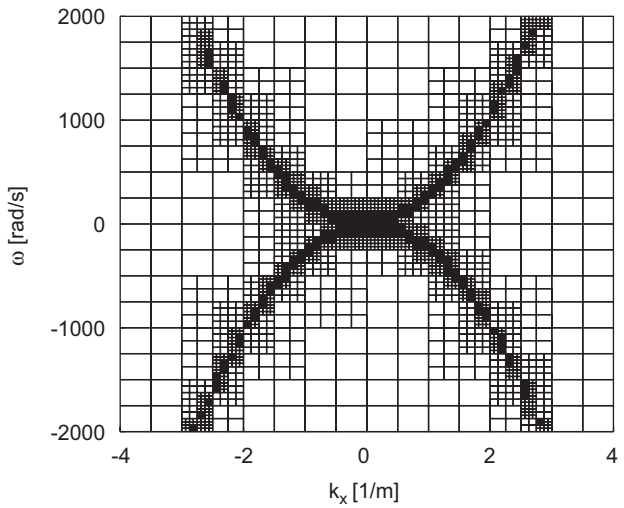

Fig. 12. Sampling grid of the system transfer function $H(k_x, \omega')$.

Due to the relatively stiff soil under consideration the influence of the tunnel structure is restricted to the direct vicinity of the tunnel, after a short distance from the tunnel the excitation of regular Rayleigh waves can be observed.

In the following the interaction of a vehicle with the coupled structure consisting of the mass–spring system mounted on a tunnel embedded in the half-space shall be investigated. The vehicle is modelled as a bogie with 5 dof as shown in Fig. 9, its parameters are given in Table 2.

An arbitrary rail surface unevenness now could be taken into account by the procedure described in Section 5. However, in the following examples two different harmonic wheel out-of-roundnesses are accounted for instead by applying the same procedure in an analogous manner, since for a linear vehicle in this case an analytical solution (that may serve as a reference solution) can be obtained. Calculations have been made for the interaction of the vehicle with a mass–spring system mounted on the tunnel embedded in the half-space and for comparison resting on a rigid foundation. The parameters for the soil can be found in Table 1 and the parameters for the tunnel shell are given in Table 3. Figs. 10 and 11 show comparisons of the wheel displacements of the two wheels due to a moving vehicle ($v = 20\,\mathrm{m/s}$) with the first and the second wheel having out-of-roundnesses with the frequencies $f = 28\,\mathrm{Hz}$ and $f = 56\,\mathrm{Hz}$, respectively, for different natural frequencies of the floating slab-track system. As expected it can be seen that the influence of the embedded

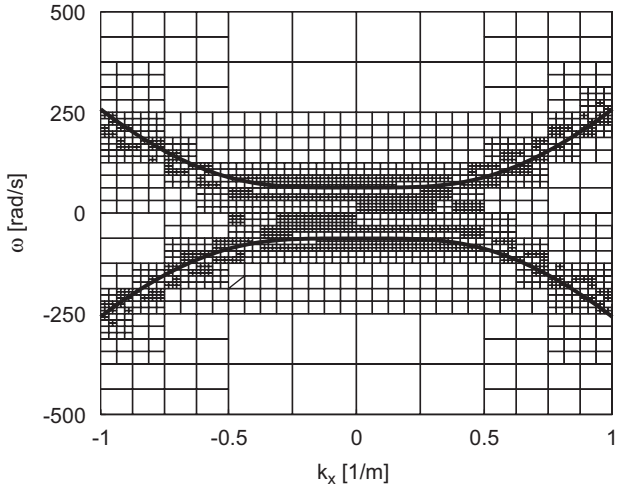

Fig. 13. Detail of the sampling grid of the system transfer function $H(k_x, \omega')$ with the analytical dispersion curve of an elastically supported beam resting on a rigid foundation (solid line).

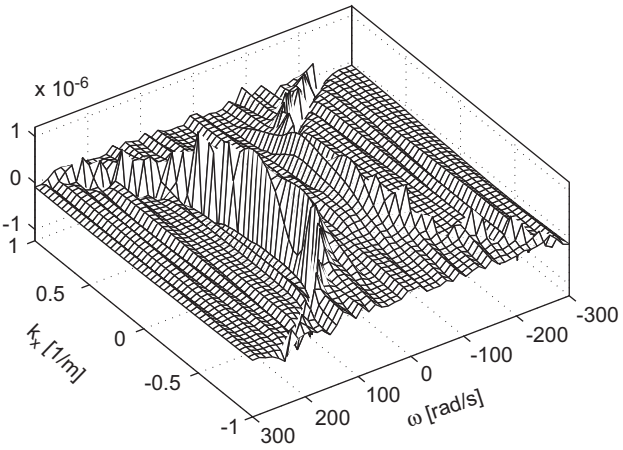

Fig. 14. Detail of the real part of the system transfer function $H(k_x, \omega')$.

tunnel compared to the elastically supported beam on rigid foundation is only low for the relatively stiff soil under consideration and lies within the accuracy of the calculation. For a mass controlled mass–spring system with the natural frequency $f = 10\,\mathrm{Hz}$ one can see the dominance of the excitation of $f = 28\,\mathrm{Hz}$ at the first wheel where a contribution of the higher frequency can hardly be seen. At the second wheel which is excited by $f = 56\,\mathrm{Hz}$ due to the increasing distance of the excitation frequency from the systems frequency the first wheel's influence now is clearly visible. For a frequency controlled mass–spring system with the natural frequency $f = 100\,\mathrm{Hz}$ the results for the complete system *slab-track– tunnel– soil* are significantly higher than the results for the elastically supported beam on rigid foundation that can be explained by the lower stiffness of a series system of two springs and a higher amplification factor with this decreasing stiffness. Here it shall be recalled that the absolute values of the displacements are shown which include the displacements of the shell. Due to the fact that now the higher excitation frequency of $f = 56\,\mathrm{Hz}$ at the second wheel is closer to the systems frequency, its influence on the first wheel now can clearly be seen. At the second wheel in this case

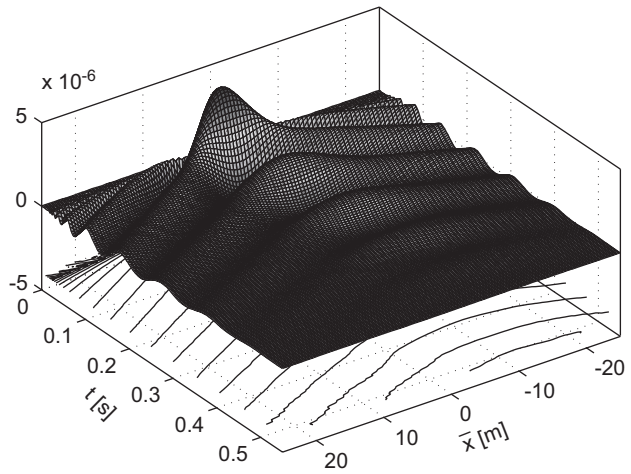

Fig. 15. Impulse response function $h(t)$.

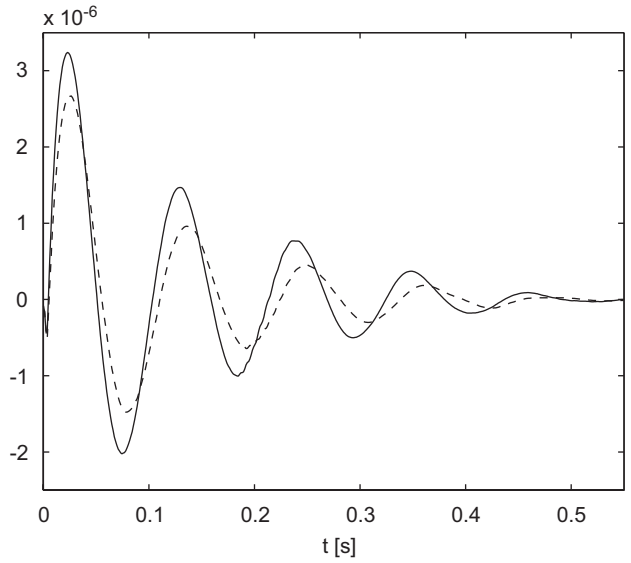

Fig. 16. Impulse response functions at $\bar{x} = -2.5\,\mathrm{m}$ (solid line) and at $\bar{x} = +2.5\,\mathrm{m}$ (dashed line).

there is no influence of the lower frequency at all because of its lower amplification factor and the higher D'Alemberts forces for the higher frequency which increase with the power of two of the frequency ω.

Fig. 11 shows similar results as Fig. 10 for different excitation frequencies at the two wheels. At the first wheel the excitation frequency now is $f = 21$ Hz, the second wheel now has a frequency due to its out-of-roundness of $f = 28$ Hz. Here the influence from one wheel's excitation frequency on the answer at the other wheel is higher due to the fact that the frequencies are closer to each other and the difference in the load as well as in the amplification function is smaller.

For the case of nonlinear primary springs of the vehicle the calculation of the interaction has to be performed in the original (x, t)-domain. Therefore the transfer function $H(\omega')$ of the complete coupled system *elastically supported plate–tunnel–half-space* has to be calculated. Figs. 12 and 13 show the grid of the adaptive sampling, Fig. 14 shows the system transfer function $H(\omega')$. As a fact of the equally spaced sampling chosen for this figure the shown function seems to be not smooth. In order to derive the impulse response function $h(t)$ an inverse transform has to be applied to the system transfer function $H(\omega')$. This task has been performed in a very efficient manner by the use of the wavelet transform as described in Refs. [39,44]. The impulse response function $h(t)$ is given in Fig. 15, the responses at $\bar{x} = \pm 2.5$ m in the moving coordinate system

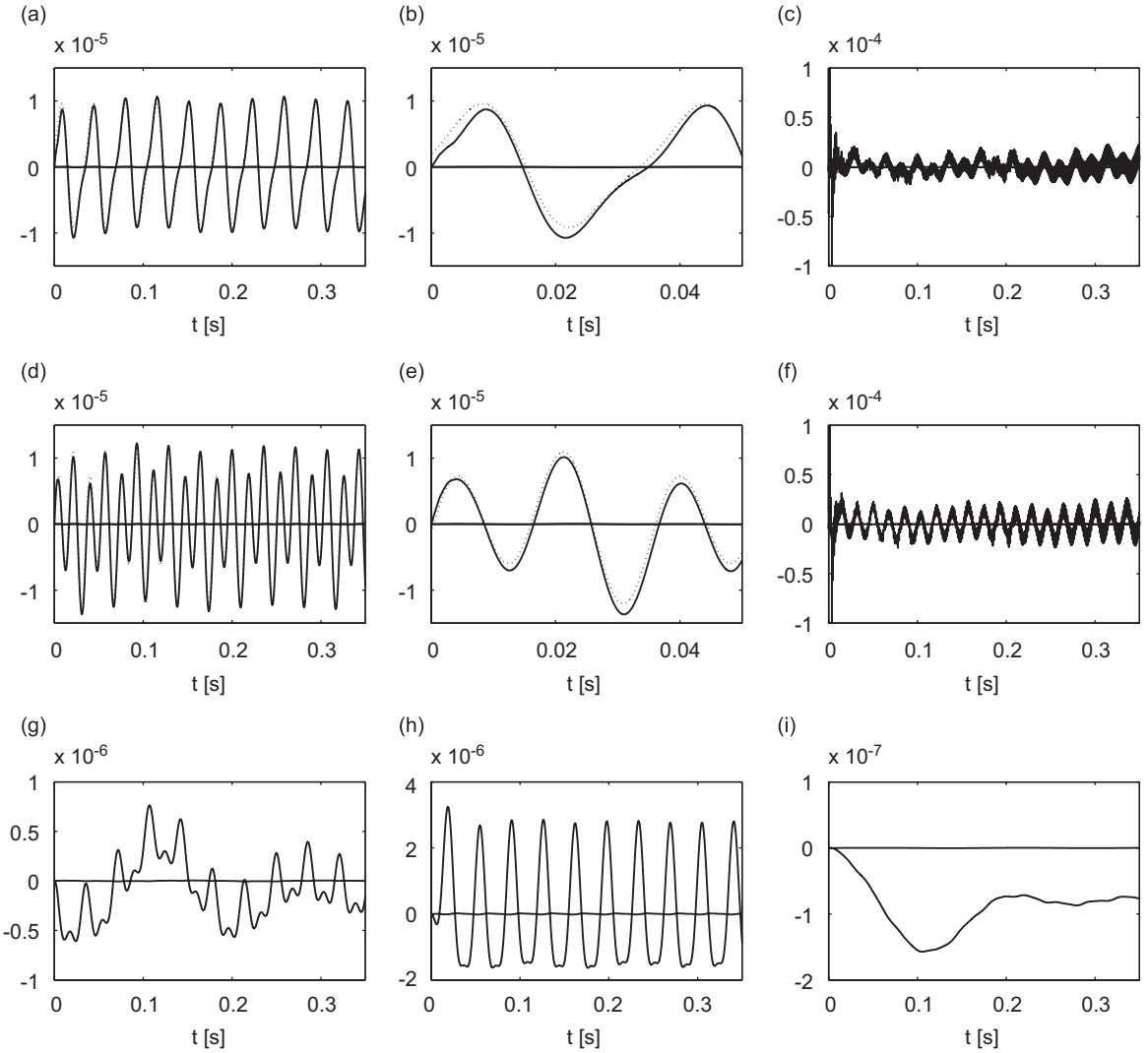

Fig. 17. Results of the nonlinear (–) and for comparison of the linear (···) calculation of the interaction ((a), (b), (d) and (e)). (a) w_{B0}, (b) w_{B0}, (c) F_0, (d) w_{B1}, (e) w_{B1}, (f) F_1, (g) w_D, (h) ϕ_D, (i) w_W.

are shown in Fig. 16. Due to the movement of the coordinate system in positive x-direction the amplitude of the beam displacement attenuates faster in this direction. Therefore in Fig. 16 the displacement at $\bar{x} = -2.5\,\mathrm{m}$ is greater than the displacement at $\bar{x} = +2.5\,\mathrm{m}$.

The nonlinear spring characteristic used for the example is given by the function

$$k_{nl} = \frac{k_0}{1 + a|w|^n} \tag{75}$$

with the parameter k_0 given in Table 2, $a = 2 \times 10^5$ and $n = 0.1$. Fig. 17 shows the solution of the nonlinear calculation for the displacements w_{B0} and w_{B1} and the interaction forces F_0 and F_1 at the first and second wheel, respectively, the displacement w_D and the rotation ϕ_D of the bogie and the displacement w_W of the coach. The time integration has been carried out applying the Newmark-β method with the parameters $\beta = 1/4$ and $\gamma = 1/2$ and the time step $\Delta t = 1.5 \times 10^{-5}$. The graphs (d) and (e) of Fig. 17 show the solutions for the displacements of the wheels, not only calculated by a time step method within the nonlinear procedure, but also calculated by a linear interaction in the frequency domain. As can be seen the solution obtained in the original time domain for the nonlinear case differs only slightly from the solution derived in frequency domain for the linear case. The effect of the nonlinear spring is only marginal.

7. Conclusions

An efficient approach to calculate the dynamic interaction of a moving vehicle with a mass–spring system mounted on a tunnel by the use of a ITM–FEM coupling has been shown. This is achieved by a combination of solutions for the uniform half-space and the continuum with cylindrical cavity in order to solve the system of a half-space with a cylindrical cavity. The tunnel structure and a portion of the surrounding soil is modelled by FEM in the Fourier transformed (k_x, y, z, ω)-domain where the coupling to the half-space with cylindrical cavity is performed. On the basis of those solutions the interaction of the mass–spring system mounted on the tunnel with a nonlinear vehicle has been shown where attention had to be paid to the problems arising in the context of RDAE.

Appendix A. Matrices $[L]$ and $[T]$ for the calculation of the displacements and the stresses in a half-space

$$[L] = \begin{bmatrix} \mathrm{i}k_x & \mathrm{i}k_x & 0 & 0 & -\lambda_2 & \lambda_2 \\ \mathrm{i}k_y & \mathrm{i}k_y & \lambda_2 & -\lambda_2 & 0 & 0 \\ \lambda_1 & -\lambda_1 & -\mathrm{i}k_y & -\mathrm{i}k_y & \mathrm{i}k_x & \mathrm{i}k_x \end{bmatrix}, \tag{76}$$

$$[T] = \mu \begin{bmatrix} -\left(2k_x^2 + \frac{\lambda}{\mu}k_p^2\right) & -\left(2k_x^2 + \frac{\lambda}{\mu}k_p^2\right) & 0 & 0 & -2\mathrm{i}k_x\lambda_2 & 2\mathrm{i}k_x\lambda_2 \\ -(2k_y^2 + \frac{\lambda}{\mu}k_p^2) & -(2k_y^2 + \frac{\lambda}{\mu}k_p^2) & 2\mathrm{i}k_y\lambda_2 & -2\mathrm{i}k_y\lambda_2 & 0 & 0 \\ (2k_r^2 - k_s^2) & (2k_r^2 - k_s^2) & -2\mathrm{i}k_y\lambda_2 & 2\mathrm{i}k_y\lambda_2 & 2\mathrm{i}k_x\lambda_2 & -2\mathrm{i}k_x\lambda_2 \\ -2k_xk_y & -2k_xk_y & \mathrm{i}k_x\lambda_2 & -\mathrm{i}k_x\lambda_2 & -\mathrm{i}k_y\lambda_2 & \mathrm{i}k_y\lambda_2 \\ 2\mathrm{i}k_y\lambda_1 & -2\mathrm{i}k_y\lambda_1 & \lambda_2^2 + k_y^2 & \lambda_2^2 + k_y^2 & -k_xk_y & -k_xk_y \\ 2\mathrm{i}k_x\lambda_1 & -2\mathrm{i}k_x\lambda_1 & k_xk_y & k_xk_y & -(\lambda_2^2 + k_x^2) & -(\lambda_2^2 + k_x^2) \end{bmatrix} \tag{77}$$

with

$$k_r = \sqrt{k_x^2 + k_y^2}. \tag{78}$$

The vector of the unknown coefficients A_j and B_{ij} is given by

$$[C]^{\mathrm{T}} = \{A_1 \mathrm{e}^{\lambda_1 z} \;\; A_2 \mathrm{e}^{-\lambda_1 z} \;\; B_{x1}\mathrm{e}^{\lambda_2 z} \;\; B_{x2}\mathrm{e}^{-\lambda_2 z} \;\; B_{y1}\mathrm{e}^{\lambda_2 z} \;\; B_{y2}\mathrm{e}^{-\lambda_2 z}\}. \tag{79}$$

Appendix B. Matrix $H(r, n, k_x, v, \omega)$ for the fundamental solution consisting of Hankel functions of the 1st kind $H_n^{(1)}$ and Hankel functions of the 2nd kind $H_n^{(2)}$

B.1. Elements of **H** *used to determine the displacement components u_r of the continuum in Eq. (30)*

$$H_{11} = \frac{n}{r} H_n^{(1)}(\alpha k_x r) - \alpha k_x H_{n+1}^{(1)}(\alpha k_x r),$$

$$H_{12} = k_x H_{n-1}^{(1)}(\beta k_x r),$$

$$H_{13} = -k_x H_{n+1}^{(1)}(\beta k_x r),$$

$$H_{14} = \frac{n}{r} H_n^{(2)}(\alpha k_x r) - \alpha k_x H_{n+1}^{(2)}(\alpha k_x r),$$

$$H_{15} = k_x H_{n-1}^{(2)}(\beta k_x r),$$

$$H_{16} = -k_x H_{n+1}^{(2)}(\beta k_x r).$$

B.2. Elements of **H** *used to determine the displacement components u_ϕ of the continuum in Eq. (30)*

$$H_{21} = \mathrm{i}\frac{n}{r} H_n^{(1)}(\alpha k_x r),$$

$$H_{22} = \mathrm{i} k_x H_{n-1}^{(1)}(\beta k_x r),$$

$$H_{23} = \mathrm{i} k_x H_{n+1}^{(1)}(\beta k_x r),$$

$$H_{24} = \mathrm{i}\frac{n}{r} H_n^{(2)}(\alpha k_x r),$$

$$H_{25} = \mathrm{i} k_x H_{n-1}^{(2)}(\beta k_x r),$$

$$H_{26} = \mathrm{i} k_x H_{n+1}^{(2)}(\beta k_x r).$$

B.3. Elements of **H** *used to determine the displacement components u_x of the continuum in Eq. (30)*

$$H_{31} = \mathrm{i} k_x H_n^{(1)}(k_x \alpha r),$$

$$H_{32} = -\mathrm{i}\beta k_x H_n^{(1)}(\beta k_x r),$$

$$H_{33} = -\mathrm{i}\beta k_x H_n^{(1)}(\beta k_x r),$$

$$H_{34} = \mathrm{i} k_x H_n^{(2)}(\alpha k_x r),$$

$$H_{35} = -\mathrm{i}\beta k_x H_n^{(2)}(\beta k_x r),$$

$$H_{36} = -\mathrm{i}\beta k_x H_n^{(2)}(\beta k_x r).$$

B.4. Elements of $\mathbf{H}$ *used to determine the stress components* $\sigma_{rr}/2\mu$ *of the continuum in Eq. (30)*

$$H_{41} = \frac{1}{r^2}\left[n(n-1) - k_x^2 r^2\left(\alpha^2 + (\alpha^2+1)\frac{\lambda}{2\mu}\right)\right]H_n^{(1)}(\alpha k_x r) + \frac{\alpha k_x}{r}H_{n+1}^{(1)}(\alpha k_x r),$$

$$H_{42} = \frac{k_x}{r}(n-1)H_{n-1}^{(1)}(\beta k_x r) - \beta k_x^2 H_n^{(1)}(\beta k_x r),$$

$$H_{43} = \frac{k_x}{r}(n+1)H_{n+1}^{(1)}(\beta k_x r) - \beta k_x^2 H_n^{(1)}(\beta k_x r),$$

$$H_{44} = \frac{1}{r^2}\left[n(n-1) - k_x^2 r^2\left(\alpha^2 + (\alpha^2+1)\frac{\lambda}{2\mu}\right)\right]H_n^{(2)}(\alpha k_x r) + \frac{\alpha k_x}{r}H_{n+1}^{(2)}(\alpha k_x r),$$

$$H_{45} = \frac{k_x}{r}(n-1)H_{n-1}^{(2)}(\beta k_x r) - \beta k_x^2 H_n^{(2)}(\beta k_x r),$$

$$H_{46} = \frac{k_x}{r}(n+1)H_{n+1}^{(2)}(\beta k_x r) - \beta k_x^2 H_n^{(2)}(\beta k_x r).$$

B.5. Elements of $\mathbf{H}$ *used to determine the stress components* $\sigma_{\phi\phi}/2\mu$ *of the continuum in Eq. (30)*

$$H_{51} = -\frac{1}{r^2}\left[n(n-1) + k_x^2 r^2(\alpha^2+1)\frac{\lambda}{2\mu}\right]H_n^{(1)}(\alpha k_x r) - \frac{\alpha k_x}{r}H_{n+1}^{(1)}(\alpha k_x r),$$

$$H_{52} = -\frac{k_x}{r}(n-1)H_{n-1}^{(1)}(\beta k_x r),$$

$$H_{53} = -\frac{k_x}{r}(n+1)H_{n+1}^{(1)}(\beta k_x r),$$

$$H_{54} = -\frac{1}{r^2}\left[n(n-1) + k_x^2 r^2(\alpha^2+1)\frac{\lambda}{2\mu}\right]H_n^{(2)}(\alpha k_x r) - \frac{\alpha k_x}{r}H_{n+1}^{(2)}(\alpha k_x r),$$

$$H_{55} = -\frac{k_x}{r}(n-1)H_{n-1}^{(2)}(\beta k_x r),$$

$$H_{56} = -\frac{k_x}{r}(n+1)H_{n+1}^{(2)}(\beta k_x r).$$

B.6. Elements of $\mathbf{H}$ *used to determine the stress components* $\sigma_{xx}/2\mu$ *of the continuum in Eq. (30)*

$$H_{61} = -k_x^2\left[(\alpha^2+1)\frac{\lambda}{2\mu} + 1\right]H_n^{(1)}(\alpha k_x r),$$

$$H_{62} = \beta k_x^2 H_n^{(1)}(\beta k_x r),$$

$$H_{63} = \beta k_x^2 H_n^{(1)}(\beta k_x r),$$

$$H_{64} = -k_x^2\left[(\alpha^2+1)\frac{\lambda}{2\mu}+1\right]H_n^{(2)}(\alpha k_x r),$$

$$H_{65} = \beta k_x^2 H_n^{(2)}(\beta k_x r),$$

$$H_{66} = \beta k_x^2 H_n^{(2)}(\beta k_x r).$$

B.7. Elements of $\mathbf{H}$ *used to determine the stress components* $\sigma_{r\phi}/2\mu$ *of the continuum in Eq. (30)*

$$H_{71} = \mathrm{i}\left[\frac{n}{r^2}(n-1)H_n^{(1)}(\alpha k_x r) - \alpha k_x \frac{n}{r}H_{n+1}^{(1)}(\alpha k_x r)\right],$$

$$H_{72} = \mathrm{i}\left[\frac{k_x}{r}(n-1)H_{n-1}^{(1)}(\beta k_x r) - \frac{1}{2}\beta k_x^2 H_n^{(1)}(\beta k_x r)\right],$$

$$H_{73} = \mathrm{i}\left[\frac{1}{2}\beta k_x^2 H_n^{(1)}(\beta k_x r) - \frac{k_x}{r}(n+1)H_{n+1}^{(1)}(\beta k_x r)\right],$$

$$H_{74} = \mathrm{i}\left[\frac{n}{r^2}(n-1)H_n^{(2)}(\alpha k_x r) - \alpha k_x \frac{n}{r}H_{n+1}^{(2)}(\alpha k_x r)\right],$$

$$H_{75} = \mathrm{i}\left[\frac{k_x}{r}(n-1)H_{n-1}^{(2)}(\beta k_x r) - \frac{1}{2}\beta k_x^2 H_n^{(2)}(\beta k_x r)\right],$$

$$H_{76} = \mathrm{i}\left[\frac{1}{2}\beta k_x^2 H_n^{(2)}(\beta k_x r) - \frac{k_x}{r}(n+1)H_{n+1}^{(2)}(\beta k_x r)\right].$$

B.8. Elements of $\mathbf{H}$ *used to determine the stress components* $\sigma_{rx}/2\mu$ *of the continuum in Eq. (30)*

$$H_{81} = \mathrm{i}\left[k_x \frac{n}{r}H_n^{(1)}(\alpha k_x r) - \alpha k_x^2 H_{n+1}^{(1)}(\alpha k_x r)\right],$$

$$H_{82} = \frac{\mathrm{i}}{2}\left[-k_x^2(\beta^2-1)H_{n-1}^{(1)}(\beta k_x r) + \beta k_x \frac{n}{r}H_n^{(1)}(\beta k_x r)\right],$$

$$H_{83} = \frac{\mathrm{i}}{2}\left[-\beta k_x \frac{n}{r}H_n^{(1)}(\beta k_x r) + k_x^2(\beta^2-1)H_{n+1}^{(1)}(\beta k_x r)\right],$$

$$H_{84} = \mathrm{i}\left[k_x \frac{n}{r}H_n^{(2)}(\alpha k_x r) - \alpha k_x^2 H_{n+1}^{(2)}(\alpha k_x r)\right],$$

$$H_{85} = \frac{\mathrm{i}}{2}\left[-k_x^2(\beta^2-1)H_{n-1}^{(2)}(\beta k_x r) + \beta k_x \frac{n}{r}H_n^{(2)}(\beta k_x r)\right],$$

$$H_{86} = \frac{\mathrm{i}}{2}\left[-\beta k_x \frac{n}{r}H_n^{(2)}(\beta k_x r) + k_x^2(\beta^2-1)H_{n+1}^{(2)}(\beta k_x r)\right].$$

B.9. Elements of $\mathbf{H}$ *used to determine the stress components* $\sigma_{\phi x}/2\mu$ *of the continuum in Eq. (30)*

$$H_{91} = -k_x \frac{n}{r} H_n^{(1)}(\alpha k_x r),$$

$$H_{92} = \frac{1}{2}\left[-k_x^2 H_{n-1}^{(1)}(\beta k_x r) + \beta k_x \frac{n}{r} H_n^{(1)}(\beta k_x r)\right],$$

$$H_{93} = \frac{1}{2}\left[\beta k_x \frac{n}{r} H_n^{(1)}(\beta k_x r) - k_x^2 H_{n+1}^{(1)}(\beta k_x r)\right],$$

$$H_{94} = -k_x \frac{n}{r} H_n^{(2)}(\alpha k_x r),$$

$$H_{95} = \frac{1}{2}\left[-k_x^2 H_{n-1}^{(2)}(\beta k_x r) + \beta k_x \frac{n}{r} H_n^{(2)}(\beta k_x r)\right],$$

$$H_{96} = \frac{1}{2}\left[\beta k_x \frac{n}{r} H_n^{(2)}(\beta k_x r) - k_x^2 H_{n+1}^{(2)}(\beta k_x r)\right].$$

References

[1] H. Grundmann, Dynamic interaction of structures with the subsoil, in: L. Frýba, J. Náprstek (Eds.), *Proceedings of the Fourth European Conference on Structural Dynamics*, *EURODYN '99*, Prag, Balkema, Rotterdam, 1999, pp. 31–41.

[2] G. Lombaert, G. Degrande, D. Clouteau, Numerical modelling of free field traffic-induced vibrations, *Soil Dynamics and Earthquake Engineering* 19 (7) (2000) 473–488.

[3] H. Grundmann, S. Lenz, Nonlinear interaction between a moving sdof system and a timoshenko beam/halfspace support, *Archive of Applied Mechanics* 72 (2003) 830–842.

[4] L. Auersch, The excitation of ground vibration by rail traffic: theory of vehicle–track–soil interaction and measurements on high-speed lines, *Journal of Sound and Vibration* 284 (1–2) (2005) 103–132.

[5] S. François, G. Lombaert, G. Degrande, Local and global shape functions in a boundary element formulation for the calculation of traffic induced vibrations, *Soil Dynamics and Earthquake Engineering* 25 (11) (2005) 839–856.

[6] L. Andersen, C. Jones, Coupled boundary and finite element analysis of vibration from railway tunnels—a comparison of two and three-dimensional models, *Journal of Sound and Vibration* 293 (3–5) (2006) 611–625.

[7] A. Karlström, A. Boström, An analytical model for train-induced ground vibrations from railways, *Journal of Sound and Vibration* 292 (1–2) (2006) 221–241.

[8] M. Steenbergen, A. Metrikine, The effect of the interface conditions on the dynamic response of a beam on a half-space to a moving load, *European Journal of Mechanics, A/Solids* 26 (1) (2007) 33–54.

[9] V. Krylov, Low-frequency ground vibrations from underground trains, *Journal of Low Frequency Noise and Vibration* 14 (1) (1995) 55–60.

[10] Q. Lin, V. Krylov, Effect of tunnel diameter on ground vibrations generated by underground trains, *Journal of Low Frequency Noise, Vibration and Active Control* 19 (1) (2000) 17–25.

[11] W. Rücker, S. Said, Influence of subway vibrations to nearby buildings; emission, transmission and protection, in: N. Chouw, G. Schmid (Eds.), *Wave Propagation and Reduction of Vibrations*, *Workshop WAVE'94*, Ruhr-Universität Bochum, Berg-Verlag, Bochum, 1994, pp. 59–78.

[12] A. Metrikine, A. Vrouwenvelder, Surface ground vibration due to a moving train in a tunnel: two-dimensional model, *Journal of Sound and Vibration* 234 (1) (2000) 43–66.

[13] C. Jones, D. Thompson, M. Petyt, Studies using a combined finite element and boundary element model for vibration propagation from railway tunnels, *Seventh International Congress on Sound and Vibration*, International Institute of Acoustics and Vibration, 2000, pp. 2703–2710.

[14] C. Jones, D. Thompson, M. Petyt, A model for ground vibration from railway tunnels, *Proceedings of the Institution of Civil Engineers, Transport* 153 (2) (2002) 121–129.

[15] M. Hussein, H. Hunt, An insertion loss model for evaluating the performance of floating slab-track for underground railway tunnels, *Proceedings of the Tenth International Congress on Sound and Vibration*, Stockholm, Schweden, 2003.

[16] M. Hussein, H. Hunt, Dynamic effect of slab discontinuity on underground moving trains, *Proceedings of the Eleventh International Congress on Sound and Vibration*, St. Petersburg, Russland, 2004, pp. 3047–3054.

[17] J. Forrest, H. Hunt, A three-dimensional tunnel model for calculation of train-induced ground vibration, *Journal of Sound and Vibration* 294 (4–5) (2006) 678–705.

[18] J. Forrest, H. Hunt, Ground vibration generated by trains in underground tunnels, *Journal of Sound and Vibration* 294 (4–5) (2006) 706–736.
[19] W. Flügge, *Stresses in Shells*, Springer, Berlin, Heidelberg, New York, 1960.
[20] L. Andersen, C. Jones, Vibration from a railway tunnel predicted by coupled finite element and boundary element analysis in two and three dimensions, in: H. Grundmann, G. Schuëller (Eds.), *Proceedings of the Fifth European Conference on Structural Dynamics, EURODYN 2002*, München, Swets & Zeitlinger, Lisse, 2002, pp. 1131–1136.
[21] X. Sheng, C. Jones, D. Thompson, Prediction of ground vibration from trains using the wavenumber finite and boundary element methods, *Journal of Sound and Vibration* 293 (3–5) (2006) 575–586.
[22] X. Sheng, C. Jones, D. Thompson, Ground vibration generated by a harmonic load moving in a circular tunnel in a layered ground, *Journal of Low Frequency Noise, Vibration and Active Control* 22 (14) (2003) 83–96.
[23] J. Luco, F. de Barros, On the three-dimensional seismic response of a class of cylindrical inclusions embedded in layered media, in: A. Cakmak, C. Brebbia (Eds.), *Soil Dynamics and Earthquake Engineering*, Vol. VI, Computational Mechanics Publications, Southampton, 1993, pp. 565–580.
[24] X. Sheng, C. Jones, D. Thompson, Modelling ground vibration from railways using wavenumber finite- and boundary-element methods, *Proceedings of the Royal Society A* 461 (2005) 2043–2070.
[25] D. Clouteau, M. Arnst, T. Al-Hussaini, G. Degrande, Freefield vibrations due to dynamic loading on a tunnel embedded in a stratified medium, *Journal of Sound and Vibration* 283 (1–2) (2005) 173–199.
[26] G. Degrande, D. Clouteau, R. Othman, M. Arnst, H. Chebli, R. Klein, P. Chatterjee, B. Janssens, A numerical model for ground-borne vibrations from underground railway traffic based on a periodic finite element-boundary element formulation, *Journal of Sound and Vibration* 293 (3–5) (2006) 645–666.
[27] D. Clouteau, M. Elhabre, D. Aubry, Periodic BEM and FEM–BEM coupling: application to seismic behaviour of very long structures, *Computational Mechanics* 25 (6) (2000) 567–577.
[28] D. Aubry, D. Clouteau, G. Bonnet, Modeling of wave propagation due to fixed or mobile dynamic sources, in: N. Chouw, G. Schmid (Eds.), *Erschütterungsausbreitung und Erschütterungsreduzierung*, *Workshop WAVE'94*, Ruhr-Universität Bochum, Berg-Verlag, Bochum, 1994, pp. 109–121.
[29] G. Degrande, M. Schevenels, P. Chatterjee, W. van de Velde, P. Hölscher, V. Hopman, A. Wang, N. Dadkah, Vibrations due to a test train at variable speeds in a deep bored tunnel embedded in London clay, *Journal of Sound and Vibration* 293 (3–5) (2006) 626–644.
[30] H. Grundmann, K. Müller, Dynamic interaction of a plate elastically mounted on a tunnel, in: C. Soize, G. Schuëller (Eds.), *Proceedings of the Sixth European Conference on Structural Dynamics*, *EURODYN 2005*, Paris, Millpress, Rotterdam, 2005, pp. 1273–1278.
[31] D. Beskos, Boundary element methods in dynamic analysis: part ii, *Applied Mechanics Reviews* 50 (3) (1997) 149–197.
[32] G. Zirwas, Ein hybrides Verfahren zur Behandlung der Bauwerk-Bodenwechselwirkung mit analytischen Integraltransformationen und numerischen Ansätzen, PhD Thesis, Lehrstuhl für Baumechanik, Mitteilungen a.d. Inst. f. Bauingw. I, Heft 10/96, TU München, 1996.
[33] J. Rastandi, Modelization of Dynamic Soil–Structure Interaction using Integral Transform-Finite Element Coupling, PhD Thesis, Lehrstuhl für Baumechanik, TU München, 2003.
[34] H. Grundmann, J. Dinkel, Moving oscillating loads acting on a dam over a layered halfspace, in: Wave 2000, 2000, pp. 53–70.
[35] K. Müller, Dreidimensionale dynamische Tunnel-Halbraum-Interaktion. Ein Verfahren auf der Grundlage einer Kopplung der Integraltransformationsmethode mit der Finite-Elemente-Methode, PhD Thesis, Lehrstuhl für Baumechanik, Schriftenreihe des Lehrstuhls für Baumechanik, Band 3, Technische Universität München, Shaker, Aachen, 2007.
[36] H. Grundmann, S. Lenz, S. Lutzenberger, Nonlinear sdof-system moving on a beam-halfspace-system, in: H. Grundmann, G. Schuëller (Eds.), *Proceedings of the Fifth European Conference on Structural Dynamics*, *EURODYN 2002*, München, Swets & Zeitlinger, Lisse, 2002, pp. 459–465.
[37] C. Long, On the completeness of the lame potentials, *Acta Mechanica* 3 (1967) 371–375.
[38] G. Müller, Ein Verfahren zur Erfassung der Fundament-Boden Wechselwirkung unter Einwirkung periodischer Lasten, PhD Thesis, Lehrstuhl für Baumechanik, Mitteilungen a.d. Inst. f. Bauingw. I, Heft 25, TU München, 1989.
[39] H. Grundmann, M. Lieb, E. Trommer, The response of a layered half-space on traffic loads moving along its surface, *Archive of Applied Mechanics* 69 (1) (1999) 55–67.
[40] A. Konrad, Der Zylinder, der zylindrische Hohlraum und die dickwandige Kreiszylinderschale unter beliebigen, ruhenden oder bewegten Lasten, PhD Thesis, Lehrstuhl für Baumechanik, Mitteilungen a.d. Institut f. Bauingw. I, Heft 17, TU München, 1985.
[41] M. Priestley, *Spectral Analysis and Time Series*, Vol. 1, Academic Press, London, 1981.
[42] H. Dietermann, A. Metrikine, The equivalent stiffness of a half-space interacting with a beam, critical velocities of a moving load along the beam, *European Journal of Mechanics* 15 (1) (1996) 67–90.
[43] S. Lutzenberger, Gekoppelte Probleme der Fahrzeug-Fahrweg Interaktion, Habilitationsschrift, Lehrstuhl für Baumechanik, TU München, 2006.
[44] H. Grundmann, E. Trommer, Transform methods - what can they contribute to (computational) dynamics?, *Computers and Structures* 79 (22–25) (2001) 2091–2102.